JCI The Journal of Clinical Investigation

Exosomes mediate sensory hair cell protection in the inner ear

Andrew M. Breglio, Lindsey A. May, Melanie Barzik, Nora C. Welsh, Shimon P. Francis, Tucker Q. Costain, Lizhen Wang, D. Eric Anderson, Ronald S. Petralia, Ya-Xian Wang, Thomas B. Friedman, Matthew J.A. Wood, Lisa L. Cunningham

J Clin Invest. 2020. https://doi.org/10.1172/JCI128867.

Research In-Press Preview **Cell biology** **Neuroscience**

Graphical abstract

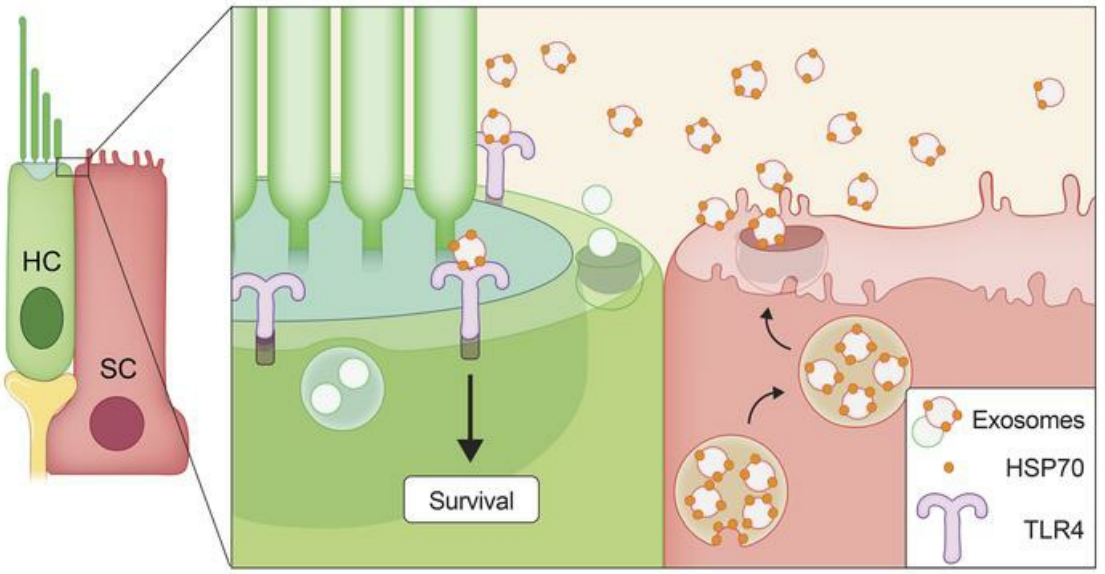

Exosomes Mediate Sensory Hair Cell Protection in the Inner Ear

Andrew M Breglio[1,2,3,4] *, Lindsey A May[1]*, Melanie Barzik[1]*, Nora C Welsh[1], Shimon P Francis[1+], Tucker Q Costain[1], Lizhen Wang[1], D Eric Anderson[5], Ronald S Petralia[1], Ya-Xian Wang[1], Thomas B Friedman[1], Matthew JA Wood[6,2], Lisa L Cunningham[1]

1. National Institute on Deafness and Other Communication Disorders, National Institutes of Health, Bethesda, MD, 20892, USA
2. Department of Physiology, Anatomy and Genetics, University of Oxford, Oxford, OX1 3QX, UK
3. Icahn School of Medicine at Mount Sinai, New York, NY, 10029, USA
4. NIH-Oxford-Cambridge Graduate Partnership Program, National Institutes of Health, Bethesda, MD, 20892, USA
5. National Institute of Diabetes and Digestive and Kidney Diseases, Bethesda, MD, 20892, USA
6. Department of Paediatrics, University of Oxford, OX3 9DU, UK

*Authors contributed equally

[+]Current Affiliation: Akouos Inc., Boston, MA 02151, USA

Corresponding author:
Lisa Cunningham
35A Convent Drive, Room 1D971
Bethesda, MD 20892
Phone: 301-443-2766
lisa.cunningham@nih.gov

Conflict of Interest

Matthew Wood is a founder and director of Evox Therapeutics.

Abstract

Hair cells are the mechanosensory receptors of the inner ear, responsible for hearing and balance. Hair cell death and consequent hearing loss are common results of treatment with ototoxic drugs, including the widely-used aminoglycoside antibiotics. Induction of heat shock proteins (HSPs) confers protection against aminoglycoside-induced hair cell death via paracrine signaling that requires extracellular HSP70 (Heat Shock 70 kDa Protein). We investigated the mechanisms underlying this non-cell-autonomous protective signaling in the inner ear. In response to heat stress, inner ear tissue releases exosomes that carry HSP70 in addition to canonical exosome markers and other proteins. Isolated exosomes from heat-shocked utricles were sufficient to improve survival of hair cells exposed to the aminoglycoside antibiotic neomycin, while inhibition or depletion of exosomes from the extracellular environment abolished the protective effect of heat shock. Hair-cell specific expression of the known HSP70 receptor, Toll-like receptor 4 (TLR4), was required for the protective effect of exosomes, and exosomal HSP70 interacted with TLR4 on hair cells. Our results indicate that exosomes are a previously undescribed mechanism of intercellular communication in the inner ear that can mediate non-autonomous hair cell survival. Exosomes may hold potential as nano-carriers for delivery of therapeutics against hearing loss.

Introduction

Disabling hearing loss affects ~6.1% of the global population (1). Most hearing loss is due to death of sensory hair cells of the inner ear. These mechanosensitive receptor cells mediate hearing and balance functions in the cochlea and vestibular organs, respectively. A variety of stresses can kill hair cells, including aging, noise trauma and clinical treatment with platinum-based cancer chemotherapeutics or aminoglycoside antibiotics, so-called “ototoxic” drugs. Ototoxic drugs cause permanent hearing loss in ~500,00 people annually in the US alone (2). In patients treated with aminoglycoside antibiotics, hearing loss is caused by direct hair cell damage. Aminoglycosides enter hair cells via both hair cell-specific membrane channels and endocytosis, resulting in intracellular accumulation and subsequent cytotoxicity (3-7). Activation of the heat stress response improves hair cell survival and preserves hearing in animal models of ototoxicity (2, 8-11). Elucidation of the mechanisms underlying this protective effect will advance both the basic science of cochlear function and the clinical development of therapies to prevent or reverse hearing loss.

Sensory hair cells are surrounded by glia-like supporting cells, named for their ability to support normal hair cell function. Supporting cells can mediate both the death and survival of hair cells (12-18). Our previous work demonstrated that supporting cells promote hair cell survival through paracrine signaling that requires extracellular Heat Shock 70 kDa Protein (HSP70) (18). Here, we tested the hypothesis that HSP70-dependent paracrine protection of hair cells is mediated by exosomes. Studies in other systems have demonstrated extracellular release of HSP70 via incorporation into exosomes (19, 20) and frequently identified HSP70 as a protein component of purified exosomes (21). Exosomes are small (50-150 nm) extracellular vesicles that are released from most cell types and can mediate intercellular communication via receptor signaling or cargo delivery to recipient cells (22). Our data indicate a crucial function for HSP70-containing exosomes in the inner ear stress response and in mediating non-cell-autonomous protection of hair cells.

Results

HSP70 is Induced in Glia-like Supporting Cells After Heat Shock

Activation of the heat stress response in the inner ear protects sensory hair cells from ototoxic drug exposure (2, 8-11), and this pro-survival effect is mediated through paracrine signaling that requires HSP70 (18). Using whole organ cultures of utricles (a vestibular organ) from adult mice, we previously demonstrated that heat shock results in HSP70 upregulation in glia-like supporting cells with negligible induction in sensory hair cells (18). Here, we confirmed induction of HSP70 in supporting cells after heat shock using additional antibodies and improved imaging methods. Utricles were heat shocked at 43˚C for 30 minutes, and upregulation of the inducible forms of HSP70 (Hspa1a and Hspa1b) was examined six hours later (Figure 1). HSP70 was induced in supporting cells with little to no induction in hair cells in both whole-mount (Figure 1A-B) and cryosectioned (Figure 1C) utricles after heat shock. These results are consistent with our previous study (18), which also demonstrated that HSP70 is secreted from heat shocked utricles. Importantly, this extracellular HSP70 was protective against hair cell death caused by the ototoxic antibiotic neomycin, thereby confirming that HSP70 acts non-cell-autonomously.

Heat Shock Induces Release of Exosomes from Inner Ear Tissue

HSP70 is secreted from many cell types via exosomes (18, 23-27). To investigate whether HSP70-dependent intercellular communication in the inner ear is facilitated by exosomes, we explored the relationship between heat stress and extracellular vesicle release. Utricles were cultured in serum-free media for 24 hours, and the utricle-conditioned media was analyzed for exosome-sized particles by nanoparticle tracking analysis (NTA), a method for real-time quantification of particles in liquids (28) (Figure 2A). Conditioned media from control utricles contained exosome-sized (~50-150 nm) particles. Heat-shock increased exosome release by 2.38-fold (95% CI = 1.74 to 2.82) (Figure 2A).

Exosomes released from heat-shocked utricles were isolated using an established procedure of differential ultracentrifugation (29, 30) (schematized in Figure 2B) and visualized by transmission electron microscopy (TEM). Consistent with previously-described exosomes from other systems (31, 32), TEM analysis of the final exosome-containing fraction showed small vesicles (90-100 nm diameter, 40-200 nm range) with a cup-shaped morphology (Figure 2C). Together, these results indicate that control utricles constitutively release exosomes, and heat shock significantly increases exosome release.

Identification of Proteins in Utricle-Derived Exosomes

Exosomes can carry a variety of cargo, such as proteins (including HSP70), lipids, and nucleic acids (21). We used tandem mass spectrometry to identify proteins associated with exosomes released from heat-shocked utricles. To yield high purity samples, exosomes were separated from soluble proteins and protein complexes in utricle-conditioned media by ultrafiltration followed by size exclusion chromatography (33). Chromatography fractions containing vesicles were analyzed as the "exosome" sample, and the remaining fractions were analyzed as the "non-exosomal fraction" sample (analogous to the supernatant resulting from purification of exosomes by ultracentrifugation). 291 protein families were identified in exosomes, only 56 of which were also present in the non-exosomal fraction (Figure 3A). A Mascot database search using the peptides that were exclusively detected in the exosome sample identified several proteins commonly enriched in exosomes (Table 1), confirming that the utricle-derived vesicles are exosomes. These established exosomal markers included tetraspanin proteins (CD9, CD63, and CD81), as well as Tumor susceptibility gene 101 (TSG101), a member of the ESCRT-I complex, and Programmed cell death 6 interacting protein/ALG-2-interacting Protein X (ALIX), an ESCRT accessory protein (reviewed in (34)). Notably, the peptide matches for members of the Heat shock 70 kDa protein family were more abundant in the exosome fraction compared to the non-exosomal fraction, suggesting that HSP70 family proteins, including the inducible forms (Hspa1a/Hspa1b), may be specifically enriched in exosomes.

Gene ontology (GO) enrichment analysis was performed on proteins identified in utricle-derived exosomes using the PANTHER Classification System (v13.1) (35, 36) followed by removing redundant ontology terms using REViGO (37). Analysis by cellular component classes identified enrichment of 35 GO terms, with the most statistically significant being "extracellular exosomes" (Figure 3B, GO:0070062). Analysis by biological process identified enrichment of 69 GO terms, with terms associated with inner ear tissue ("sensory perception of sound", GO:0007605; "sensory perception of mechanical stimulus", GO:0050954) being among the top five statistically significant results (Figure 3C).

The integrin family of transmembrane adhesion receptors controls various fundamental cellular functions, including proliferation and cell survival (38, 39). Integrins are heterodimers comprised of an

alpha and beta subunit. In exosomes, integrins are embedded in the membrane where they mediate intercellular communication. Specifically, the complement of exosomal integrins specifies the target organs or cell types with which an exosome interacts (40). Three alpha subunits (alpha 3, alpha 7, and alpha V) and one beta subunit (beta 1) were identified in exosomes from utricles, suggesting that they may specify exosomal tropism in the inner ear (Table 2).

Isolated Exosomes Improve Hair Cell Survival

We next investigated whether the HSP70-carrying exosomes are protective against aminoglycoside-induced hair cell death. Cultured utricles were heat shocked, and exosomes were purified from conditioned media via differential ultracentrifugation (Figure 4A). Both the pelleted exosome fraction and the non-exosomal supernatant fraction (containing extracellular, soluble proteins and nucleic acids not associated with exosomes) were tested for their ability to protect hair cells from ototoxicity. Treatment of recipient utricles with the aminoglycoside antibiotic neomycin killed approximately 48% of hair cells (Figure 4B-C). Application of utricle-derived exosomes significantly reduced neomycin-induced hair cell death while the non-exosomal (supernatant) fraction was not protective (Figure 4B-C). Thus, utricle-derived exosomes are protective against aminoglycoside-induced hair cell death.

Exosome Biogenesis is Required for the Protective Effect of Heat Shock

The necessity of exosomes for the protective effect of heat stress was examined through pharmacological inhibition of exosome biogenesis. Exosomes are generated as intraluminal vesicles that bud into a multivesicular body; a process that requires the sphingolipid ceramide (Figure 5A) (41). Spiroepoxide is a selective and irreversible inhibitor of neutral sphingomyelinase II, the enzyme that catalyzes cellular production of ceramide (42, 43). NTA of conditioned media revealed that spiroepoxide resulted in a significant decrease in the number of exosomes released by heat-shocked utricles (0.5×10^9 vs. 1.5×10^9 exosomes/ml) (Figure 5B). Importantly, neither heat shock alone nor heat shock in the presence of spiroepoxide resulted in hair cell death relative to control utricles (Figure 5C). Therefore, the reduced quantity of exosomes released from spiroepoxide-treated utricles cannot be attributed to cell death. We next used spiroepoxide to determine if exosome biogenesis is required for the pro-survival effect of heat

shock in utricles. Neomycin killed approximately 40% of hair cells, while heat shock significantly improved hair cell survival. Notably, inhibition of exosome biogenesis using spiroepoxide abolished the protective effect of heat shock (Figure 5D). Thus, ceramide is necessary for the formation of utricular exosomes, and inhibition of ceramide production using spiroepoxide inhibits exosome release from cultured utricles. Together these data demonstrate that the hair cell protection induced by heat stress in utricles requires exosomes.

Supporting Cells Produce More Exosomes Compared to Hair Cells

We next investigated the cellular source(s) of protective exosomes in the utricle. Utricles contain several cell types, predominantly sensory hair cells and glia-like supporting cells. Additional cell types include macrophages, fibroblasts, and transitional epithelium. A differential fluorescent labeling approach was used to determine the contributions of hair cells and supporting cells to the total exosome population (Figure 6A). mTmG global double-fluorescent reporter mice express membrane-targeted (myristoylated) tandem dimer Tomato (mtdTomato) protein in all cells, and myristoylated green fluorescent protein (mGFP) following Cre-mediated excision of mtdTomato (44). Myristoylation of both fluorophores results in their incorporation into lipid membranes, including exosome membranes. NTA of conditioned media from heat-shocked mTmG utricles and utricles of age-matched control (WT) mice verified that lipid modification of the fluorophores did not interfere with exosome production or release (Figure 6B). mTmG mice were crossed with mice expressing Cre recombinase under control of the growth factor independent 1 (Gfi1) promoter to generate mice in which 96% of hair cells expressed mGFP, while all other cell types expressed mtdTomato (Figure 6C). An established microscopy-based technique (45, 46) was used to detect and quantify fluorescent exosomes. This method does not rely on resolving exosomes, which are below the resolution limit of a standard confocal microscope (~200 nm); instead it allows detection of exosome-associated fluorescent proteins (mtdTomato or mGFP). The size of the fluorescent puncta (Airy disks) sampled on the microscope's photodetector is not equivalent to the size of the exosomes but instead is related to the fluorescence intensity of the point source. Using this method, 17.4% ± 1.8 (mean ± SEM) exosomes purified from heat-shocked utricles from mTmG mice crossed to *Gfi1*-Cre mice were identified as mGFP-positive, indicating they originated from hair cells (Figure 6C-F). In the complementary

experiment, mTmG mice were crossed with mice expressing tamoxifen-inducible Cre recombinase (CreER) under the control of the glial high-affinity glutamate transporter (GLAST, *Slc1a3*) to produce mice in which 65% of supporting cells expressed mGFP, while all other cell types expressed mtdTomato (Figure 6G). 25.3% ± 2.0 of exosomes isolated from these utricles after heat shock were mGFP-positive (i.e., originated from supporting cells) (Figure 6H-J). Adjusting for the efficiency of recombination by the two Cre lines (96% efficiency for *Gfi1*-Cre; 65% efficiency for *GLAST*-CreER), reveals that ~18% of utricle-derived exosomes originated from hair cells, ~38% from supporting cells, and ~44% from other cell types including macrophages, fibroblasts, and transitional epithelium (Figure 6K). These data demonstrate that both hair cells and supporting cells release exosomes, with supporting cells releasing about twice as many exosomes as hair cells.

Heat Shock Protein 70 is Required for the Pro-Survival Effect of Exosomes

We previously reported that extracellular HSP70 is required for the protective effect of heat shock against neomycin-induced hair cell death (18). Here, we show that 1) HSP70 is associated with utricle-derived exosomes (Table 1), 2) exosomes are essential for the protective response induced by heat stress (Figure 4B-C, Figure 5D), and 3) the non-exosomal fraction is not protective (Figure 4B-C). Together, these data support the hypothesis that exosome-associated HSP70 is required for the heat-shock-induced pro-survival effect.

To directly test this hypothesis, we first confirmed HSP70 distribution by Western Blot analysis (Figure 7A). Exosomes and the non-exosomal supernatant fraction were isolated from heat-shocked utricles by differential ultracentrifugation (Figure 2B), and the macromolecules in the non-exosomal fraction were further concentrated using a centrifugal filtration device (3,000 MWCO). Total protein concentrations for each sample were determined using a bicinchoninic acid (BCA) assay. When equivalent protein amounts were analyzed by Western blot, HSP70 and the canonical exosome marker CD81 were exclusively detected in exosomes and were absent from the non-exosomal fraction. These data are in agreement with our proteomics analyses (Table 1) and indicate that HSP70 released from utricles is exosome-associated.

We next used immunoelectron microscopy to visualize exosomal HSP70. Exosomes from heat-shocked utricles showed positive immunogold labeling for HSP70, with gold particles clustered around the exosome membrane (Figure 7B-C). Control samples treated with only the gold-conjugated secondary antibody showed no HSP70 immunoreactivity (data not shown). These results confirm our proteomics and Western blot data demonstrating that utricle-derived exosomes carry HSP70 (Table 1), and they suggest that HSP70 is associated with the exosomal membrane, either directly by integration into the lipid bilayer or indirectly by forming complexes with transmembrane proteins, as has been reported for HSP70 in exosomes from other systems (26, 47-50).

A function-blocking antibody against HSP70 (51, 52) was used to investigate whether exosome-associated HSP70 is required for the protective effect of exosome application (Figure 7D). Utricles exposed to neomycin showed significant death of hair cells, which was again reduced by the application of isolated exosomes. This protective effect was abolished when isolated exosomes were pre-treated with a function-blocking antibody against HSP70. The HSP70 function-blocking antibody alone had no effect on hair cell survival (Figure 7D). These data indicate that HSP70 is critical for the protective effect of exosomes, and that HSP70 is at least partially exposed on the exosome surface, where it is accessible by the anti-HSP70 antibody.

To examine whether non-exosomal HSP70 is sufficient for protection, we applied soluble HSP70 to neomycin-treated utricles (Figure 7E). A stringent quantification of hair cell density was employed by manually counting surviving hair cells in the entire posterior region of treated utricles (average area: 80,000 μm^2). While application of exosomes isolated from heat-shocked utricles again improved hair cell survival in neomycin-treated utricles, addition of exogenous HSP70, (i.e. HSP70 *not* associated with exosomes), was not protective (Figure 7E). These results indicate that association of HSP70 with exosomes is required to induce a pro-survival response in hair cells, and they imply that additional exosomal properties and/or cargo also contribute to the protective effect of exosome application.

Together, our data indicate that HSP70 is associated with the membrane of utricle-derived exosomes, and that this exosomal HSP70 is required for the protective effect of exosomes against neomycin-induced hair cell death.

Exosomes Interact with Toll-Like Receptor 4 on Hair Cells

Extracellular HSP70 is an endogenous ligand of toll-like receptor 4 (TLR4) (53-56). Binding of HSP70 to TLR4 mediates protection from ischemia-reperfusion injury in cardiomyocytes and from lethal hyperoxic lung injury (57-59). We therefore explored the role of TLR4 signaling in exosome-mediated hair cell protection in utricles exposed to ototoxic stress. To specifically investigate whether TLR4 is required in hair cells, B6(Cg)-*Tlr4*$^{tm1.1Karp}$/J ("TLR4-loxP") mice were crossed with B6.Cg-*Tg(Atoh1-cre)1Bfri/J* mice expressing Cre recombinase under control of atonal bHLH transcription factor 1 (Atoh1, *Atoh1*) ("Atoh1-Cre") to produce offspring in which TLR4 was conditionally deleted from hair cells ("TLR4 cKO mice"). In utricles from littermate control mice (B6(Cg)-*Tlr4*$^{tm1.1Karp}$xB6.Cg; "WT"), the application of exosomes from heat-shocked utricles improved hair cell survival following neomycin exposure (Figure 8A), similar to our data from CBA/J mice (Figure 4B-C). However, when applied to TLR4 cKO utricles, exosomes did not improve hair cell survival in the presence of neomycin. These results indicate that exosome-mediated protection requires TLR4 expression in hair cells.

A proximity ligation assay (PLA) was used to assess whether HSP70 and TLR4 interact in utricles. Two proteins are detected using primary antibodies from different species, which are subsequently visualized using secondary antibodies conjugated to short DNA oligonucleotides. If the two antigen-antibody complexes are in proximity (30-40 nm apart), the conjugated DNA oligonucleotides participate in rolling circle PCR amplification. The DNA product is visualized with labeled oligonucleotide probes to mark the sites of protein-protein interaction. The well-characterized interaction between HSP70 and its co-chaperone HSP40 was used as a positive control paradigm to validate PLA in utricles. Punctate fluorescence, indicating HSP70-HSP40 interaction, was detectable in control utricles, and the number of HSP70-HSP40 puncta increased after heat shock (Figure 8B, E). Similarly, a baseline number of puncta was observed for the interaction of HSP70 with TLR4 under control conditions, and the number of puncta increased significantly after heat shock (Figure 8B, F). Importantly, this heat shock-induced increase in HSP70-TLR4 puncta was abolished in the presence of two different HSP70 function-blocking antibodies (fbAb), but not in the presence of control IgG (Fig 8B, F), confirming the specificity of the HSP70-TLR4 interaction.

To further corroborate that HSP70 specifically interacts with TLR4 on hair cells, we used PLA to examine the HSP70-TLR4 interaction in utricles from TLR4 cKO mice. As expected, puncta indicating interaction were observed for both HSP70-HSP40 (positive control) as well as HSP70-TLR4 in wild-type utricles (Figure 8C). Both of these interactions increased significantly after heat shock (Figure 8C). In contrast, interaction between HSP70 and TLR4 was not detected above background in TLR4 cKO mice in either control or heat shock conditions (Figure 8C, G). Together, these data demonstrate that exosomal HSP70 interacts with TLR4 at the hair cell surface, and the specificity of this interaction is confirmed by our data that either blockade of HSP70 or genetic deletion of TLR4 from hair cells abolishes this interaction.

Discussion

Exosomes are Mediators of the Heat Stress Response in the Inner Ear

Our data reveal a biological function for exosomes in the inner ear. Previous work has shown that activation of the heat stress response improves hair cell survival in the face of toxic stress. We present evidence that exosomes are critical intercellular mediators of the protective effect of heat shock against aminoglycoside-induced hair cell death. Heat stress induced exosome release in the inner ear, consistent with data in other systems showing that heat stress impacts both the quantity of exosomes released and their HSP content (26, 27, 60). Consequently, our analyses of utricle-derived exosomes by TEM and tandem mass spectrometry revealed that they share both morphology and common protein markers with exosomes from other systems (reviewed by (31) and (61)).

Two lines of experimentation demonstrate the critical roles of exosomes in non-cell-autonomous protection in the inner ear. First, utricle-derived exosomes protected against neomycin-induced hair cell death, while the non-exosomal fraction of the conditioned media was not protective. This was not due to a general increase of global protein abundance in the exosomal fraction, since both our proteomics data and our BCA analyses indicate 5-10 fold higher total protein content in the supernatant fraction compared to the exosomal fraction (data not shown). Second, inhibition of neutral sphingomyelinase II using spiroepoxide demonstrated that exosome biogenesis is required for the protective effect of heat shock. Thus, our data indicate that exosomes are both necessary and sufficient for protection against hair cell death caused by neomycin.

Inner Ear Exosomes carry Heat Shock Protein 70

Extracellular HSP70 promotes survival of hair cells exposed to ototoxic drugs; however, the mechanism by which HPS70 is secreted has been unclear (18). Our data indicate that HSP70 is released from inner ear cells by incorporation into exosomes. We detected HSP70 in isolated exosomes via tandem mass spectrometry, Western blot, and immunoelectron microscopy. By immunoelectron microscopy, HSP70 appears to be associated with the exosomal membrane. This idea is further supported by the observation that incubation of purified exosomes with a function-blocking antibody against HSP70 abolished their protective activity, suggesting that HSP70 is at least partially exposed on the exosome surface and thus

accessible for antibody binding. Our results join the growing body of literature demonstrating HSP70 secretion via exosomes (20, 23, 62, 63). Exosomal HSP70 affects target cell protein homeostasis (64), and HSP70 on the exosomal surface has repeatedly been implicated in immune cell activation, particularly in the context of cancer (26, 47-50, 63). Notably, functional exosome-associated HSP70 appears to be important for interaction with immediate downstream receptor(s) in the inner ear, since antibodies against HSP70 inhibited the HSP70-TLR4 interaction in hair cells (Figure 8). This finding is in agreement with data in myeloid-derived suppressive cells, where targeting membrane-associated HSP70 with an aptamer blocked the ability of exosomes to bind to toll-like receptor 2 (TLR2) (65).

This work identifies exosome-associated HSP70 as an indispensable factor for hair cell survival in the presence of ototoxic drugs. In addition, our proteomics analysis identified numerous other proteins associated with exosomes released from heat-shocked utricles, some of which may have key roles in the pro-survival activity of inner ear exosomes.

Model for Exosome-Mediated Protection of Hair Cells

Our data are consistent with a model in which utricle-derived exosomes carry surface-associated HSP70, and this exosomal HSP70 interacts with TLR4 on hair cells to promote their survival (Figure 9). Though our data suggest that significantly more exosomes are derived from supporting cells relative to hair cells, extremely limited exosome yield from mouse utricle explants precludes sorting and analyzing subpopulations of exosomes according to their cell type of origin. Given that the isolated exosomes in this study represent the total population of exosomes released from all cells of the utricle, it is unclear if the exosomes that promote hair cell survival are specifically those released by supporting cells. However, our previous work (18) as well as data presented here (Figure 1) show that heat stress induces HSP70 primarily in supporting cells, and thus it seems reasonable to posit that HSP70-positive exosomes may be released by this cell type.

Our data show that exosomes interact with TLR4 on hair cells, but the pro-survival signaling events downstream of this interaction remain unknown. The pro-survival activity of exosomal HSP70 may be independent of HSP70's chaperone function, as has been demonstrated in hyperoxia-induced lung injury, where extracellular HSP70 acts as a TLR4 ligand to exert a cytoprotective effect both in endothelial

cells and in lung tissue (59). Of interest, the protective mechanism of HSP70-containing inner ear exosomes displays similarities to cardioprotection by plasma-derived exosomes carrying HSP70. Here, surface-associated exosomal HSP70 interacts with TLR4 on cardiomyocytes, stimulating downstream signaling kinases ERK1/2 and p38 MAPK and activating Heat Shock Protein Family B (Small) Member 1 (HSPB1, *HSP27*). This exosome-driven, HSP70-TLR4-induced signaling cascade protects cardiomyocytes against ischemia-reperfusion injury (58, 66). A similar mechanism may underlie the protective effect of exosomes against hair cell death. Ongoing analysis of the transcriptomic changes induced in exosome-treated hair cells may illuminate the pro-survival responses within hair cells.

Exosomes as Inner Ear Therapeutics

Death of sensory hair cells is the central event leading to permanent hearing loss caused by ototoxic drugs, noise exposure, and aging (67, 68). Identification of the mechanisms that promote hair cell survival will inform the rational design of therapies to prevent hearing loss. Here we present evidence that exosomes mediate intercellular communication in the inner ear and protect against ototoxicity. Thus, exosomes may represent a means of clinical intervention to protect hair cells in vivo during cellular stress. Future experiments will determine if exosome-mediated hair cell protection extends to protection against other ototoxic stressors.

We identified the protein cargo of utricle-derived exosomes using tandem mass spectrometry and demonstrated that HSP70 is a critical component of this exosomal cargo (Figure 7D, 8B). These data may allow for the scalable production of hair-cell-protective exosomes in vitro. Exosomes have garnered significant interest in recent years for the therapeutic delivery of proteins, nucleic acids, and small molecules (69-73), and our data indicate that they may be leveraged as nanocarriers to deliver therapeutics to treat inner ear disorders. In contrast to viral and non-viral delivery systems, exosomes have the advantages of a large packaging capacity, biocompatibility, non-immunogenicity, and the innate ability to cross biological membranes, including the blood-brain barrier (61). Like the brain, the inner ear is separated from systemic circulation by a semipermeable, multi-component barrier (blood-labyrinth barrier) (74, 75). Engineered exosomes can deliver designer cargo to the brain following systemic administration (76). Similar results may be achievable in the inner ear using specific targeting proteins identified in our

proteomic analysis. The complement of integrins on exosomes determines their tissue tropism in other systems (40). Integrin subunits, alpha-3, alpha-7, alpha-V, and beta-1 were detected in our proteomics analysis, and their assembly into heterodimers may direct exosomes to specific inner ear cell types. Exosomes may also increase the delivery efficiency of locally-administered inner ear therapies, as has been demonstrated for exosome-associated adeno-associated virus (AAV), which improved hair cell infectivity as compared to naked AAV (77).

Taken together, our results indicate that exosomes represent a previously undescribed mechanism of intercellular communication in the inner ear that can mediate non-autonomous survival signaling and protect sensory hair cells against lethal stresses. Exosomes may be engineered to deliver therapeutic molecules to the inner ear to prevent or reverse hearing loss.

Methods

Mice. 4-8 week old CBA/J mice (Jackson Laboratory, Stock No. 000656) were used as controls throughout except in experiments using Toll-like receptor 4 (TLR4) conditional knockout mice, where either littermates or C57BL/6J mice (as indicated) were used as controls. Approximately equal numbers of male and female mice were used in each experiment.

Transgenic *ROSA26*$^{mT/mG}$ mice (*Gt(ROSA)26Sor*$^{tm4(ACTB-tdTomato,-EGFP)Luo}$/J, Jackson Laboratory, Stock No. 007676), referred to as "mTmG" mice, were used for visualization of extracellular vesicles. These Cre-reporter mice express membrane-targeted (myristoylated) tandem dimer Tomato (mtdTomato) prior to Cre recombination, and myristoylated green fluorescent protein (mGFP) after Cre-mediated excision of tdTomato (44). Both fluorophores are myristoylated, promoting their ubiquitous insertion into membranes. To differentially label extracellular vesicles derived from hair cells and supporting cells, two complementary breeding schemes were used. To label hair cells with mGFP and supporting cells with mtdTomato, hair cell-specific *Gfi1*$^{Cre/+}$ mice (generated by Dr. Lin Gan, University of Rochester and generously provided by Dr. Ronna Hertzano, University of Maryland) were used. *Gfi1*$^{Cre/+}$ mice express Cre recombinase in the GFI1 locus, which is required for hair cell differentiation and survival (78). Offspring were backcrossed to *ROSA26*$^{mTmG/mTmG}$ to produce *Gfi1*$^{Cre/+}$; *ROSA26*$^{mTmG/mTmG}$ mice. To label supporting cells with mGFP and hair cells with mtdTomato, supporting cell-specific *GLAST*-CreER mice (Tg(Slc1a3-cre/ERT)1Nat, Jackson Laboratory, Stock No. 012586) were used. *GLAST*-CreER mice express tamoxifen-inducible Cre recombinase under the control of the glial high affinity glutamate transporter (GLAST) promoter (79). *GLAST*-CreER; *ROSA26*$^{mTmG/+}$ offspring were backcrossed to *ROSA26*$^{mTmG/mTmG}$ mice to obtain *GLAST*-CreER; *ROSA26*$^{mTmG/mTmG}$ offspring. Cre recombination was induced at P21 by intraperitoneal injection of tamoxifen (0.225 mg/g body weight; Sigma-Aldrich). Cre recombination efficiency was established by crossing either *Gfi1*-Cre mice or *GLAST*-CreER mice to a transgenic reporter mouse line (B6.Cg-*Gt(ROSA)26Sor*$^{tm14(CAG-tdTomato)Hze}$/J; Jackson Laboratory, Stock No. 007914) and quantification of tdTomato-positive hair cells (*Gfi1*-Cre, 96% recombination efficiency) or tdTomato-positive supporting cells (*GLAST*-CreER, 65% recombination efficiency) in utricle explants (80).

Hair-cell specific TLR4 conditional knockout mice were generated by crossing B6.Cg-*Tg(Atoh1-cre)1Bfri/J* mice (Jackson Laboratory, Stock No. 011104) with B6(Cg)-*Tlr4*$^{tm1.1Karp}$*/J* mice (Jackson

Laboratory, Stock No. 024872). In B6.Cg-*Tg(Atoh1-cre)1Bfri/J* mice, the mouse atonal homolog 1 (Atoh1) regulatory sequences direct Cre recombinase expression in all hair cells and a small percentage of supporting cells (81). B6(Cg)-*Tlr4*$^{tm1.1Karp}$/J mice contain loxP sites flanking exon 3 of the *Tlr4* gene. Offspring that inherited the *Atoh1*-Cre transgene had *Tlr4* conditionally deleted from hair cells and are referred to as "TLR4 cKO" mice. Offspring that did not inherit the *Atoh1*-Cre transgene were used as littermate controls.

Utricle Culture. Explanted mouse utricles were used as an in vitro preparation of inner ear hair cells and supporting cells. Mice were euthanized by CO_2 inhalation followed by decapitation. Utricles were excised and cultured as previously described (82, 83). Briefly, the bony labyrinth was removed, placed into Medium 199 (Gibco) at 37°C, and utricles were dissected under sterile conditions before transfer into 1 ml complete medium (DMEM/F12 with phenol red (Gibco), 5 % heat-inactivated FBS (Gibco), 50 U/ml Penicillin G (Sigma-Aldrich)). Utricles were cultured overnight in a 24-well tissue culture plate at 37°C and 5% CO_2 prior to any experimental manipulation.

As FBS contains large numbers of exosomes (84), experiments in which vesicles were to be isolated and/or analyzed were performed in serum-free culture medium (DMEM/F12, 50 U/ml Penicillin G). Utricles initially cultured in serum-containing media were rinsed and transferred to serum-free medium. Imaging of fluorescently-labeled exosomes was performed in serum-free medium without phenol red.

Heat Shock: utricles and their culture medium (1 ml) were transferred to sterile microcentrifuge tubes and placed into a 43°C water bath for 30 minutes. Control (no heat shock) utricles were transferred to microcentrifuge tubes and placed in the incubator at 37°C for 30 minutes. Following incubation, all utricles were transferred to complete medium in a tissue culture plate and returned to the incubator under standard culture conditions for two hours.

Nanoparticle tracking analysis. Nanoparticle tracking analysis (NTA) using a NanoSight NS300 controlled by NTA software version 3.1 (Malvern Panalytical) was used to measure the concentration and size distribution of extracellular vesicles. Samples were pushed through a fluidics flow chamber at a constant flow rate using a syringe pump (Harvard Apparatus). The scattered light from vesicles illuminated with a 488 nm laser was recorded at 30 frames per second using a sCMOS camera three

times for 60 seconds (Figure 2A, Figure 5B) or five times for 30 seconds (Figure 6B). The camera sensitivity for each capture was kept identical within the same experiment (15 - Figure 2A, Figure 5B; 13 - Figure 6B). The detection threshold for particle analysis was set at 3.

Exosome Purification. Samples were of two categories: 1) minimally processed conditioned media or 2) purified and concentrated exosomes. Minimally processed conditioned media was analyzed to characterize the total population of EVs released from utricles (Figure 2A, Figure 6B). To remove large particles and cellular debris prior to NTA, conditioned medium was processed either by centrifugation (2,000 x g for 10 minutes; Figure 2A) or filtration (0.2 µm syringe filter; Figure 6B).

Exosomes were purified from conditioned medium by either ultracentrifugation or size-exclusion chromatography (SEC). Ultracentrifugation provided higher yield and was used for most experiments. SEC was used to generate high-purity samples for proteomic analyses (Figure 3, Tables 1-2).

Ultracentrifugation Method: Exosomes were isolated from utricle-conditioned medium using an abbreviated version of a previously described protocol (29). Cells and large cellular debris were removed by centrifugation (300 x g, 10 minutes, 4°C), followed by sedimentation of large vesicles and additional cellular debris (10,000 x g, 30 minutes, 4°C). Exosomes were pelleted by subjecting the supernatant from the second spin to a high-speed centrifugation step (100,000 x g, 70 minutes, 4°C) in polycarbonate tubes (349622) using a TLA-100.3 rotor and an Optima MAX-XP ultracentrifuge (Beckman Coulter). The exosome pellet was resuspended in PBS or culture medium by trituration with a micropipette.

Exosomes for proteomic analysis were purified by ultrafiltration and SEC. Cellular debris and large vesicles were removed from conditioned medium by filtration through a PVDF syringe filter (Millex Durapore, 0.22 µm, Millipore Sigma). Vesicles were concentrated using a centrifugal concentrator (5,000 molecular weight cut-off (MWCO), Vivaspin Turbo 15, Sartorius VS15T11) at 3,000 x g. The concentrated sample (250-500 µl) was separated on a Superose 6 Increase 10/300 GL SEC column (equilibrated with PBS, pH 7.4) using an ÄKTA pure 25 chromatography system (both GE Healthcare Life Sciences) at 4°C. A constant flow rate of 0.5 ml/min was maintained throughout and UV absorbance (280 nm) was continuously recorded. Eluted sample fractions were collected every 1 ml for column volumes 0-1 and every 2 ml for column volumes 1-1.5. Exosome-containing fractions were identified according to the UV absorption and by NTA of each fraction. The exosomal and non-exosomal fractions (containing secreted

proteins and protein complexes) were separately pooled and concentrated using centrifugal concentrators (3,000 MWCO, Vivaspin Turbo 15, Sartorius VS15T91) prior to proteomic analysis.

Transmission Electron Microscopy and Immunoelectron Microscopy. Transmission electron microscopy (TEM) was used to visualize purified utricle exosomes. Fixation and embedding were performed as previously described (29). Briefly, isolated exosomes were resuspended in 2% paraformaldehyde (PFA), deposited as droplets onto Formvar-carbon coated grids and rinsed in PBS before fixation in 1% glutaraldehyde. Samples were rinsed in ddH_2O, contrasted in uranyl-oxalate solution (pH 7), and embedded in 2% methyl cellulose and 4% uranyl acetate at a ratio of 9:1. Excess solution was blotted on filter paper and grids were air dried.

Immunoelectron microscopy was used to visualize the association of HSP70 with utricle-derived exosomes. Exosomes were fixed and deposited on Formvar-carbon coated grids. Grids were rinsed twice by placing them on a 100 µl drop of PBS, followed by two washes in 50 mM glycine in PBS. Samples were blocked in 5% BSA (A3294, Sigma) in PBS for 10 min prior to incubation with an HSP70 antibody (SC-33575, Santa Cruz Biotechnology) diluted 1:5 in blocking solution for 2 hours. Control samples were incubated in blocking solution alone. Samples were rinsed three times in wash buffer (0.1% BSA in PBS). Secondary staining was performed for 30 min using 10 nm gold-conjugated goat anti-rabbit IgG F(ab')2 (H+L) antibody (15731, BBI Solutions/Ted Pella) diluted 1:40 in blocking solution. Samples were rinsed four times in PBS, fixed in 1% glutaraldehyde in PBS and rinsed four times in ddH_2O. Samples were contrasted and embedded as described above.

Images were collected using a JEM-2100 transmission electron microscope (JEOL) equipped with an Orius SC1000B camera (Gatan) and DigitalMicrograph software. Post-acquisition processing was performed in ImageJ2 (85).

Tandem Mass Spectrometry. 160 utricles were dissected and cultured in DMEM/F12 medium supplemented with 50 U/ml of Penicillin G and G-5 serum-free supplement (Thermo Fisher) as a chemically defined substitute for FBS. Utricles were heat-shocked, and exosomes were purified from conditioned media via the SEC-based method described above. Samples were flash-frozen in liquid nitrogen and stored at -80°C. Samples were essentially processed and analyzed as in normal high-

sensitivity bottom-up proteomics using sodium dodecanoate (86) with post-extraction clean-up using STAGE tips (87).

Raw data were abstracted to the mgf format using MSConvert from the ProteoWizard 3.0.6839 package. These files were entered in the Mascot search engine against the MaxQuant common contaminants database (Max Planck Institute of Biochemistry) and the SWISS-PROT protein sequence databases for *Homo sapiens, Mus musculus*, and *Pichia pastoris* (02-27-2018 release). Gene Ontology (GO) term enrichment analyses were performed in Protein Analysis Through Evolutionary Relationships (PANTHER) version 13.1 (35, 36). Redundancy within lists of enriched GO terms was minimized using Reduce and Visualize Gene Ontology (REViGO) (37) with similarity set to 0.5.

Modeling Ototoxicity In Vitro. Utricles were treated with neomycin to induce hair cell death. Neomycin sulfate solution (140 mg/ml, VetOne) was added to culture medium to a final concentration of 2.5 mM. Neomycin-containing culture medium was equilibrated in the incubator (37°C, 5% CO_2) for at least two hours prior to use.

Application of Exogenous Exosomes. 20 to 24 utricles were cultured, heat-shocked, and transferred to serum-free culture medium. Conditioned medium was collected 24 hours later and processed via differential ultracentrifugation as described above, resulting in a pellet containing exosomes and a supernatant containing extracellular macromolecules not associated with exosomes, “non-exosomal fraction”. The exosome pellet was resuspended in serum-free neomycin-containing medium to create “neomycin + exosomes” culture medium. Neomycin was added to the non-exosomal fraction to create “neomycin + non-exosomal fraction” culture medium. Culture media were allowed to equilibrate for two hours in the incubator. Following equilibration, freshly dissected utricles were transferred to each culture medium and incubated for 24 hours, then fixed and processed as detailed below.

Pharmacologic Inhibition of Exosome Biogenesis. Utricles were treated with spiroepoxide (282108-77-4, Santa Cruz Biotechnology), an inhibitor of neutral sphingomyelinase II (N-SMase), to inhibit exosome biogenesis. N-SMase catalyzes production of ceramide, which is necessary for exosome production in some systems (41). Spiroepoxide was dissolved in DMSO and added to culture medium at a final concentration of 0.375 μM. Simultaneous exposure to neomycin and spiroepoxide was performed by addition of both drugs to the culture medium, followed by equilibration of the media for two hours, after

505 which utricles were incubated with the media for 24 hours. Control utricles were exposed to DMSO
506 (vehicle control). After 24 hours, utricles were fixed and processed as detailed below.

507 **Immunohistochemistry and Confocal Microscopy**. Utricles were fixed in 4% PFA in PBS for 30
508 minutes at room temperature and were then incubated for 2 hours at room temperature in blocking
509 solution (0.5% Triton X-100, 2% BSA, and 0.8% normal goat serum (NGS) in PBS). Hair cells were
510 labeled overnight at 4°C with mouse-anti-Myosin VIIa antibody (1:100, MYO7A 138-1, Developmental
511 Studies Hybridoma Bank), followed by Alexa Fluor 546-conjugated goat-anti-mouse IgG (1:500,
512 Invitrogen) for 4 hours at room temperature. F-actin was labeled with Alexa Fluor 647 Phalloidin (1:60,
513 Molecular Probes) for 45 minutes at room temperature, and nuclei were stained with Hoechst 33342
514 (1:500, both Molecular Probes) for 5 minutes. All incubation steps were performed in blocking solution.

515 Labeled utricles were mounted in Fluoromount-G (Southern Biotech) and imaged using a 40x 1.4
516 N.A. Plan-Apochromat oil objective and an Axiovert 200M inverted microscope with a confocal scan head
517 (LSM780) equipped with a GaAsP detector and controlled by Zen software (all Zeiss). All samples were
518 imaged under identical acquisition settings. Surviving hair cells within the extrastriolar region of each
519 utricle were counted manually within five regions of interest (ROIs) and averaged to reflect the mean hair
520 cell density per utricle. For consistency throughout the manuscript, hair cell density was normalized to the
521 average hair cell count per 900 μm^2 utricle area (except Figure 7E).

522 **Quantification of Labeled Exosomes**. Utricles from *Gfi1*$^{Cre/+}$; *ROSA26*$^{mTmG/+}$ and tamoxifen-treated
523 *GLAST-CreER*; *ROSA26*$^{mTmG/mTmG}$ mice (described above) had differentially-labeled hair cells and
524 supporting cells. The membrane-associated reporter fluorophores incorporate into exosomes and report
525 the cell type of origin of a particular exosome. The relative abundance of fluorescent hair cell- and
526 supporting cell-derived EVs in conditioned medium from heat-shocked *Gfi1*$^{Cre/+}$; *ROSA26*$^{mTmG/+}$ utricles
527 was determined using laser scanning confocal microscopy.

528 Utricles (n = 9-11 per biological replicate) were dissected, heat-shocked, rinsed, and transferred
529 to 40 µl of phenol red-free, serum-free medium in a 96-well tissue culture plate. Conditioned medium was
530 collected 24 hours later, and cellular debris was removed by centrifugation (10,000 x g, 10 minutes). The
531 exosome-containing supernatant was imaged using a 63x 1.4 N.A. Plan-Apochromat oil objective and an
532 Axiovert 200M inverted microscope with a confocal scan head (LSM780) controlled by Zen software (all

Zeiss) as previously described (45, 46). Briefly, a 10 µl droplet was placed on a 35 mm glass coverslip-bottomed culture dish (MatTek) and covered. Two sequential images of exosomes adherent to the coverslip were captured with the mtdTomato signal imaged first and the mGFP second. Image acquisition was reversed for the next two images to account for potential photobleaching. For each sample, a second 10 µl exosome droplet was imaged using the same parameters, resulting in eight images per sample.

Using ImageJ2, images were split into separate channels, smoothed, and threshold was applied manually. Thresholding settings were kept constant for all images in an experiment. Exosomes in each channel were automatically quantified using the Analyze Particles function, with the minimum particle area set to 2 pixels^2, and no circularity restrictions (0.00-1.00). Resulting exosome counts in each channel were averaged across the eight images collected for each sample. The experiment was repeated three times.

Western Blot Analyses. 22 utricles were cultured, heat-shocked, and transferred to serum-free culture medium. Conditioned culture medium was collected 24 hours later and processed via differential ultracentrifugation (see Exosome Purification), resulting in a pellet containing the exosomes, and supernatant containing extracellular proteins not associated with exosomes. The exosome-depleted supernatant was further concentrated with a centrifugal filter unit (3,000 MWCO; Millipore) at 4,000 x g and 4˚C. Both the concentrated non-exosomal supernatant and the purified exosomes were processed as follows: Samples were resuspended in 1x RIPA lysis buffer (Millipore) supplemented with cOmplete mini EDTA-free protease inhibitor cocktail (Roche), vortexed for 1 minute and denatured at 95˚C for 5 min in 1x Laemmli buffer (Bio-Rad). Protein concentration was analyzed using a BCA protein assay kit (Thermo Fisher), using half of each sample. The remaining sample was denatured at 95˚C for 5 min in 1x Laemmli buffer and subjected to SDS-PAGE using NuPAGE 4-12% Bis-Tris gels followed by protein transfer to a 0.45-µm pore PVDF membrane (both Thermo Fisher). Membranes were blocked in 1% BSA in TBS with 0.1% Tween 20 (TBS-T). Washes were performed with TBS-T. All antibodies were diluted in 1% BSA in TBS-T. Primary antibodies: HSPA1 (Thermo Fisher PA5-28003, 1:500) and CD81 (Cell Signaling D5O2Q, 1:500). Horseradish Peroxidase (HRP)-linked secondary antibody: Anti-rabbit IgG (Cell Signaling 7074S, 1:10,000). Membranes were incubated with 2% NaN3 between primary antibodies to inactivate HRP (88).

Protein bands were visualized by chemiluminescence using SuperSignal West Femto Duration Substrate (Thermo Fisher) and a ChemiDoc MP Imaging System (Bio-Rad).

HSP70 Function-Blocking Antibody. Utricles (n = 40-44) were cultured and processed as described above (Western Blot Analyses) to generate a pellet containing the exosomes and supernatant containing extracellular macromolecules not associated with exosomes. The pelleted exosome fraction was resuspended in serum-free neomycin-containing medium to create “neomycin + exosomes” culture medium. This medium was equilibrated for two hours in the incubator and was divided into two 1-ml aliquots. Rabbit anti-HSP70/HSC70 (SC-33575, H-300, Santa Cruz Biotechnology) was added at a concentration of 1 µg/ml to one aliquot to create “neomycin + exosomes + HSP70 fbAb” culture medium. Control medium was prepared by adding anti-HSP70/HCS70 antibody at the same concentration to equilibrated, serum-free, neomycin-containing culture medium (“neomycin + HSP70 fbAb”). Naïve utricles were transferred to each experimental culture medium and incubated for 24 hours, then fixed, stained, and imaged as above (Immunohistochemistry and Confocal Microscopy).

Application of Exogenous HSP70. 22 utricles were cultured and processed as above (Western Blot Analyses) to generate a pellet containing the exosomes. The pelleted exosomes were resuspended in serum-free neomycin-containing culture medium to create “neomycin + exosome” culture medium. Recombinant human HSP70 (5 µg; ADI-ESP-555, Enzo) was resuspended in serum-free neomycin-containing culture medium to create “neomycin + HSP70” culture medium. Culture media was equilibrated for two hours at 37°C. Naïve utricles were transferred to each experimental culture medium and incubated for 24 hours, after which they were fixed, stained, and imaged as detailed above (Immunohistochemistry and Confocal Microscopy). Quantification was performed by counting surviving hair cells in the entire posterior region of treated utricles followed by normalization of hair cell counts to utricle area.

Proximity Ligation Assay. A Duolink proximity ligation assay (DUO92014, Sigma) was used to visualize interaction between HSP70 and TLR4. Utricles from TLR4 cKO or WT control mice were heat shocked. Six hours later, utricles were fixed in 3% PFA for 30 minutes, rinsed in PBS, permeabilized with 0.1% Triton X-100 in PBS for 10 minutes, rinsed in PBS, and blocked (2% BSA + 10% NGS in PBS) for three hours at room temperature. Utricles were incubated overnight at 4°C with mouse-anti-HSP70 antibody

(C92F3A-5) and rabbit-HSP40 antibody (ADI-SPA-400-F, both Enzo) (control) or mouse-anti-HSP70 antibody (C92F3A-5, Enzo) and rabbit-anti-TLR4 antibody (MAB27591, R&D Systems). HSP70 was blocked with either rabbit-HSPA1A antibody (PA5-28003, Thermo Fisher) or rabbit-HSP70 antibody (SC33575, H-300, Santa Cruz Biotechnology), using rabbit IgG isotype (31325, Thermo Fisher) as control. Antibodies were used at a final concentration of 1 µg/ml. One utricle per well was transferred to Nunc MiniTrays (136528, Thermo Fisher) and treated according to the manufacturer's instructions. Briefly, utricles were incubated in secondary solution (15 µl) containing anti-rabbit PLUS and anti-mouse MINUS probes for one hour at 37°C. Utricles were rinsed and incubated in ligation solution (15 µl) for 30 minutes at 37°C, rinsed and incubated in amplification solution (15µl) for 100 minutes at 37°C. After a final wash step, F-actin was labeled with Alexa Fluor 488 Phalloidin (1:50), and nuclei were stained with Hoechst 33342 (1:15,000, both Molecular Probes) in PBS for 30 minutes at room temperature. Utricles were imaged using either a 60x lambda 1.4 N.A. Plan-Apochromat oil objective or a 60x TIRF 1.49 N.A. Plan-Apochromat oil objective and an Eclipse Ti-E inverted microscope with a hybrid confocal scan head (resonant and galvano; A1R HD) equipped with a GaAsP detection unit controlled by NIS-Elements C software (all Nikon); or a 63x 1.4 N.A. DIC Plan-Apochromat oil objective and an Axiovert 200M inverted microscope with a confocal scan head (LSM780) equipped with an Airyscan detection unit controlled by Zen software (all Zeiss). Identical settings for pinhole, gain, and offset were used between samples on each microscope. Acquired Airyscan datasets were processed using Zen Desk software (Zeiss). All datasets were processed for PLA puncta quantification in ImageJ as follows: Image channels were separated and a maximum z projection of the z sections containing the PLA signal was performed. Threshold was applied manually, and PLA puncta were automatically quantified using the Analyze Particles function, with the minimum particle area set to 0.2 - 1 μm^2 and no circularity restrictions (0.00-1.00). Puncta were counted for 2-3 ROIs per utricle, averaged across the utricle and normalized to a 1,000 μm^2 area.

Statistics. All statistical analyses were performed using Prism 8 (GraphPad) software. The Shapiro-Wilks test was used to analyze datasets for normality. For multiple comparisons, statistical significance was determined by one-way analysis of variance (ANOVA) followed by the Holm-Šídák multiple comparisons test (89) for data with equal variances and with Brown-Forsythe and Welsh ANOVA followed by Dunnett's

T3 multiple comparisons test otherwise. Comparisons of multiple groups with independent variables was performed by two-way ANOVA followed by the Holm-Šídák multiple comparisons test. Statistical tests are indicated in each figure legend. Data are presented as mean ± SEM throughout. Statistical significance is indicated throughout the manuscript as: (*) $P < 0.05$, (**) $P < 0.01$, (***) $P < 0.001$, (****) $P < 0.0001$.

Study Approval. All animal procedures were approved by the NIDCD/NINDS Animal Care and Use Committee (protocol #1327).

Author Contributions

AB, LM, MW, and LC conceived the project. AB, LM, MB, NW, SF, and LC planned the experiments. AB, LM, NW, SF, TC, LW, DA, RP, YW and MB performed the experiments and interpreted the data. AB, MB and LC wrote the manuscript with input from all authors. TF, MW, and LC supervised the project.

The assignment of the authorship order for the first three authors on this manuscript is essentially chronological: AB started the project and worked in close collaboration with LM, who designed and performed several of the critical experiments. Together they produced the first submitted version of the manuscript. After AB and LM left the laboratory, MB completed additional important experiments, performed extensive new analyses and re-wrote the manuscript.

Acknowledgements

We are grateful to Imre Mäger and Samir El Andaloussi for guidance regarding exosome purification and analysis techniques. We thank Erina He for illustrations in Figures 1D, 5A, 6C, 6G, and 9. We thank Matthew Kelley and Wade Chien for helpful comments on the manuscript. This research was supported by the Division of Intramural Research of the National Institute on Deafness and Other Communication Disorders (project numbers 1ZIADC000079, 1ZICDC000081 to L.L.C. and DC000039 to T.B.F.).

References

1. WorldHealthOrganization. WHO Global Estimates on Prevalence of Hearing Loss. https://www.who.int/deafness/estimates/en/. Updated 2018. Accessed April 3, 2019.
2. Francis SP, et al. Celastrol inhibits aminoglycoside-induced ototoxicity via heat shock protein 32. *Cell Death Dis.* 2011;2:e195.
3. Francis SP, et al. A novel role of cytosolic protein synthesis inhibition in aminoglycoside ototoxicity. *J Neurosci.* 2013;33(7):3079-3093.
4. Hailey DW, et al. Fluorescent aminoglycosides reveal intracellular trafficking routes in mechanosensory hair cells. *J Clin Invest.* 2017;127(2):472-486.
5. Huth ME, et al. Mechanisms of aminoglycoside ototoxicity and targets of hair cell protection. *Int J Otolaryngol.* 2011;2011:937861.
6. Marcotti W, et al. The aminoglycoside antibiotic dihydrostreptomycin rapidly enters mouse outer hair cells through the mechano-electrical transducer channels. *J Physiol.* 2005;567(Pt 2):505-521.
7. Warchol ME. Cellular mechanisms of aminoglycoside ototoxicity. *Curr Opin Otolaryngol Head Neck Surg.* 2010;18(5):454-458.
8. Yoshida N, et al. Heat stress and protection from permanent acoustic injury in mice. *J Neurosci.* 1999;19(22):10116-10124.
9. Cunningham LL, and Brandon CS. Heat shock inhibits both aminoglycoside-and cisplatin-induced sensory hair cell death. *J Assoc for Res Otolaryngol.* 2006;7(3):299-307.
10. Taleb M, et al. Hsp70 inhibits aminoglycoside-induced hair cell death and is necessary for the protective effect of heat shock. *J Assoc Res Otolaryngol.* 2008;9(3):277-289.

11. Baker TG, et al. Heat shock protein-mediated protection against Cisplatin-induced hair cell death. *J Assoc Res Otolaryngol.* 2015;16(1):67-80.

12. Hawkins J. *Otophysiology*. Karger Publishers; 1973:125-141.

13. Bohne BA, and Rabbitt KD. Holes in the reticular lamina after noise exposure: implication for continuing damage in the organ of Corti. *Hear Res.* 1983;11(1):41-53.

14. Forge A. Outer hair cell loss and supporting cell expansion following chronic gentamicin treatment. *Hear Res.* 1985;19(2):171-182.

15. Leonova EV, and Raphael Y. Organization of cell junctions and cytoskeleton in the reticular lamina in normal and ototoxically damaged organ of Corti. *Hear Res.* 1997;113(1-2):14-28.

16. Bird JE, et al. Supporting cells eliminate dying sensory hair cells to maintain epithelial integrity in the avian inner ear. *J Neurosci.* 2010;30(37):12545-12556.

17. Monzack EL, et al. Live imaging the phagocytic activity of inner ear supporting cells in response to hair cell death. *Cell Death Differ.* 2015;22(12):1995-2005.

18. May LA, et al. Inner ear supporting cells protect hair cells by secreting HSP70. *J Clin Invest.* 2013;123(8):3577-3587.

19. Mambula SS, and Calderwood SK. Heat shock protein 70 is secreted from tumor cells by a nonclassical pathway involving lysosomal endosomes. *J Immunol.* 2006;177(11):7849-7857.

20. De Maio A. Extracellular Hsp70: export and function. *Curr Protein Pept Sci.* 2014;15(3):225-231.

21. Kim DK, et al. EVpedia: a community web portal for extracellular vesicles research. *Bioinformatics.* 2015;31(6):933-939.

22. Colombo M, et al. Biogenesis, secretion, and intercellular interactions of exosomes and other extracellular vesicles. *Annu Rev Cell Dev Biol.* 2014;30:255-289.

23. Lancaster GI, and Febbraio MA. Exosome-dependent trafficking of HSP70: a novel secretory pathway for cellular stress proteins. *J Biol Chem.* 2005;280(24):23349-23355.

24. Peinado H, et al. Melanoma exosomes educate bone marrow progenitor cells toward a pro-metastatic phenotype through MET. *Nat Med.* 2012;18(6):883-891.

25. Takeuchi T, et al. Intercellular chaperone transmission via exosomes contributes to maintenance of protein homeostasis at the organismal level. *Proc Natl Acad Sci U S A.* 2015;112(19):E2497-E2506.

26. Lv LH, et al. Anticancer drugs cause release of exosomes with heat shock proteins from human hepatocellular carcinoma cells that elicit effective natural killer cell antitumor responses in vitro. *J Biol Chem.* 2012;287(19):15874-15885.

27. Clayton A, et al. Induction of heat shock proteins in B-cell exosomes. *J Cell Sci.* 2005;118(Pt 16):3631-3638.

28. Filipe V, et al. Critical evaluation of Nanoparticle Tracking Analysis (NTA) by NanoSight for the measurement of nanoparticles and protein aggregates. *Pharm Res.* 2010;27(5):796-810.

29. Thery C, et al. Isolation and characterization of exosomes from cell culture supernatants and biological fluids. *Curr Protoc Cell Biol.* 2006;Chapter 3:Unit 3 22.

30. Gardiner C, et al. Techniques used for the isolation and characterization of extracellular vesicles: results of a worldwide survey. *J Extracell Vesicles.* 2016;5:32945.

31. Wu Y, et al. Exosomes: improved methods to characterize their morphology, RNA content, and surface protein biomarkers. *Analyst.* 2015;140(19):6631-6642.

32. Raposo G, and Stoorvogel W. Extracellular vesicles: exosomes, microvesicles, and friends. *J Cell Biol.* 2013;200(4):373-383.

33. Nordin JZ, et al. Ultrafiltration with size-exclusion liquid chromatography for high yield isolation of extracellular vesicles preserving intact biophysical and functional properties. *Nanomedicine.* 2015;11(4):879-883.

34. Kowal J, et al. Biogenesis and secretion of exosomes. *Curr Opin Cell Biol.* 2014;29:116-125.

35. Mi H, et al. PANTHER version 11: expanded annotation data from Gene Ontology and Reactome pathways, and data analysis tool enhancements. *Nucleic Acids Res.* 2017;45(D1):D183-D189.

36. Thomas PD, et al. PANTHER: a library of protein families and subfamilies indexed by function. *Genome Res.* 2003;13(9):2129-2141.

37. Supek F, et al. REVIGO summarizes and visualizes long lists of gene ontology terms. *PLoS One.* 2011;6(7):e21800.

38. Zutter MM. Integrin-mediated adhesion: tipping the balance between chemosensitivity and chemoresistance. *Adv Exp Med Biol.* 2007;608:87-100.

39. Hynes RO. Integrins: bidirectional, allosteric signaling machines. *Cell.* 2002;110(6):673-687.

40. Hoshino A, et al. Tumour exosome integrins determine organotropic metastasis. *Nature.* 2015;527(7578):329-335.

41. Trajkovic K, et al. Ceramide triggers budding of exosome vesicles into multivesicular endosomes. *Science.* 2008;319(5867):1244-1247.

42. Hannun YA. Functions of ceramide in coordinating cellular responses to stress. *Science.* 1996;274(5294):1855-1859.

43. Arenz C, and Giannis A. Synthesis of the First Selective Irreversible Inhibitor of Neutral Sphingomyelinase. *Angew Chem Int Ed Engl.* 2000;39(8):1440-1442.

44. Muzumdar MD, et al. A global double-fluorescent Cre reporter mouse. *Genesis.* 2007;45(9):593-605.

45. Heusermann W, et al. Exosomes surf on filopodia to enter cells at endocytic hot spots, traffic within endosomes, and are targeted to the ER. *J Cell Biol.* 2016;213(2):173-184.

46. Lai CP, et al. Visualization and tracking of tumour extracellular vesicle delivery and RNA translation using multiplexed reporters. *Nat Commun.* 2015;6:7029.

47. Gastpar R, et al. Heat shock protein 70 surface-positive tumor exosomes stimulate migratory and cytolytic activity of natural killer cells. *Cancer Res.* 2005;65(12):5238-5247.

48. Vega VL, et al. Hsp70 translocates into the plasma membrane after stress and is released into the extracellular environment in a membrane-associated form that activates macrophages. *J Immunol.* 2008;180(6):4299-4307.

745 49. Cho JA, et al. MHC independent anti-tumor immune responses induced by Hsp70-
746 enriched exosomes generate tumor regression in murine models. *Cancer Lett.*
747 2009;275(2):256-265.
748 50. Chalmin F, et al. Membrane-associated Hsp72 from tumor-derived exosomes mediates
749 STAT3-dependent immunosuppressive function of mouse and human myeloid-derived
750 suppressor cells. *J Clin Invest.* 2010;120(2):457-471.
751 51. Roué G, et al. Cyclin D1 mediates resistance to apoptosis through upregulation of
752 molecular chaperones and consequent redistribution of cell death regulators.
753 *Oncogene.* 2008;27:4909.
754 52. Li C-J, et al. MAPK pathway mediates EGR-1-HSP70-dependent cigarette smoke-induced
755 chemokine production. *American Journal of Physiology-Lung Cellular and Molecular*
756 *Physiology.* 2007;292(5):L1297-L1303.
757 53. Jheng HF, et al. Albumin stimulates renal tubular inflammation through an HSP70-TLR4
758 axis in mice with early diabetic nephropathy. *Dis Model Mech.* 2015;8(10):1311-1321.
759 54. Vabulas RM, et al. HSP70 as endogenous stimulus of the Toll/interleukin-1 receptor
760 signal pathway. *J Biol Chem.* 2002;277(17):15107-15112.
761 55. Luong M, et al. Stimulation of TLR4 by recombinant HSP70 requires structural integrity
762 of the HSP70 protein itself. *J Inflamm (Lond).* 2012;9:11.
763 56. Asea A, et al. Novel signal transduction pathway utilized by extracellular HSP70: role of
764 toll-like receptor (TLR) 2 and TLR4. *J Biol Chem.* 2002;277(17):15028-15034.

765 57. de Oliveira AA, et al. Unveiling the Interplay between the TLR4/MD2 Complex and
766 HSP70 in the Human Cardiovascular System: A Computational Approach. *Int J Mol Sci.*
767 2019;20(13).
768 58. Vicencio JM, et al. Plasma exosomes protect the myocardium from ischemia-reperfusion
769 injury. *J Am Coll Cardiol.* 2015;65(15):1525-1536.
770 59. Zhang Y, et al. A protective Hsp70-TLR4 pathway in lethal oxidant lung injury. *J Immunol.*
771 2013;191(3):1393-1403.
772 60. Chen T, et al. Chemokine-containing exosomes are released from heat-stressed tumor
773 cells via lipid raft-dependent pathway and act as efficient tumor vaccine. *J Immunol.*
774 2011;186(4):2219-2228.
775 61. E. L. Andaloussi S, et al. Extracellular vesicles: biology and emerging therapeutic
776 opportunities. *Nat Rev Drug Discov.* 2013;12(5):347-357.
777 62. De Maio A, and Vazquez D. Extracellular heat shock proteins: a new location, a new
778 function. *Shock.* 2013;40(4):239-246.
779 63. Elsner L, et al. The heat shock protein HSP70 promotes mouse NK cell activity against
780 tumors that express inducible NKG2D ligands. *J Immunol.* 2007;179(8):5523-5533.
781 64. Takeuchi T, et al. Intercellular chaperone transmission via exosomes contributes to
782 maintenance of protein homeostasis at the organismal level. *Proc Natl Acad Sci U S A.*
783 2015;112(19):E2497-2506.
784 65. Gobbo J, et al. Restoring Anticancer Immune Response by Targeting Tumor-Derived
785 Exosomes With a HSP70 Peptide Aptamer. *J Natl Cancer Inst.* 2016;108(3).

66. Davidson SM, et al. Cardioprotection mediated by exosomes is impaired in the setting of type II diabetes but can be rescued by the use of non-diabetic exosomes in vitro. *J Cell Mol Med.* 2018;22(1):141-151.
67. Furness DN. Molecular basis of hair cell loss. *Cell Tissue Res.* 2015;361(1):387-399.
68. Lanvers-Kaminsky C, et al. Drug-induced ototoxicity: Mechanisms, Pharmacogenetics, and protective strategies. *Clin Pharmacol Ther.* 2017;101(4):491-500.
69. Batrakova EV, and Kim MS. Using exosomes, naturally-equipped nanocarriers, for drug delivery. *J Control Release.* 2015;219:396-405.
70. Bunggulawa EJ, et al. Recent advancements in the use of exosomes as drug delivery systems. *Journal of Nanobiotechnology.* 2018;16(1):81.
71. Conlan RS, et al. Exosomes as Reconfigurable Therapeutic Systems. *Trends Mol Med.* 2017;23(7):636-650.
72. Murphy DE, et al. Extracellular vesicle-based therapeutics: natural versus engineered targeting and trafficking. *Exp Mol Med.* 2019;51(3):32.
73. van Dommelen SM, et al. Microvesicles and exosomes: opportunities for cell-derived membrane vesicles in drug delivery. *J Control Release.* 2012;161(2):635-644.
74. Neng L, et al. Endothelial cell, pericyte, and perivascular resident macrophage-type melanocyte interactions regulate cochlear intrastrial fluid-blood barrier permeability. *J Assoc Res Otolaryngol.* 2013;14(2):175-185.
75. Zhang W, et al. Perivascular-resident macrophage-like melanocytes in the inner ear are essential for the integrity of the intrastrial fluid-blood barrier. *Proc Natl Acad Sci U S A.* 2012;109(26):10388-10393.

76. Alvarez-Erviti L, et al. Delivery of siRNA to the mouse brain by systemic injection of targeted exosomes. *Nat Biotechnol.* 2011;29(4):341-345.

77. Gyorgy B, et al. Rescue of Hearing by Gene Delivery to Inner-Ear Hair Cells Using Exosome-Associated AAV. *Mol Ther.* 2017;25(2):379-391.

78. Matern M, et al. Gfi1(Cre) mice have early onset progressive hearing loss and induce recombination in numerous inner ear non-hair cells. *Sci Rep.* 2017;7:42079.

79. Heng JS, et al. Hypoxia tolerance in the Norrin-deficient retina and the chronically hypoxic brain studied at single-cell resolution. *Proc Natl Acad Sci U S A.* 2019;116(18):9103-9114.

80. Stone JS, et al. Characterization of Adult Vestibular Organs in 11 CreER Mouse Lines. *J Assoc Res Otolaryngol.* 2018;19(4):381-399.

81. Yang H, et al. Generation and characterization of Atoh1-Cre knock-in mouse line. *Genesis.* 2010;48(6):407-413.

82. Cunningham LL. The adult mouse utricle as an in vitro preparation for studies of ototoxic-drug-induced sensory hair cell death. *Brain Res.* 2006;1091(1):277-281.

83. Brandon CS, et al. Dissection of adult mouse utricle and adenovirus-mediated supporting-cell infection. *J Vis Exp.* 2012(61).

84. Shelke GV, et al. Importance of exosome depletion protocols to eliminate functional and RNA-containing extracellular vesicles from fetal bovine serum. *J Extracell Vesicles.* 2014;3.

85. Schindelin J, et al. The ImageJ ecosystem: An open platform for biomedical image analysis. *Mol Reprod Dev.* 2015;82(7-8):518-529.

86. Lin Y, et al. Sodium laurate, a novel protease- and mass spectrometry-compatible detergent for mass spectrometry-based membrane proteomics. *PLoS One.* 2013;8(3):e59779.

87. Rappsilber J, et al. Protocol for micro-purification, enrichment, pre-fractionation and storage of peptides for proteomics using StageTips. *Nat Protoc.* 2007;2(8):1896-1906.

88. Kaufmann SH. Reutilization of immunoblots after chemiluminescent detection. *Anal Biochem.* 2001;296(2):283-286.

89. Holm S. A simple sequentially rejective multiple test procedure. *Scand J Statist.* 1979:65-70.

Figures and Figure legends

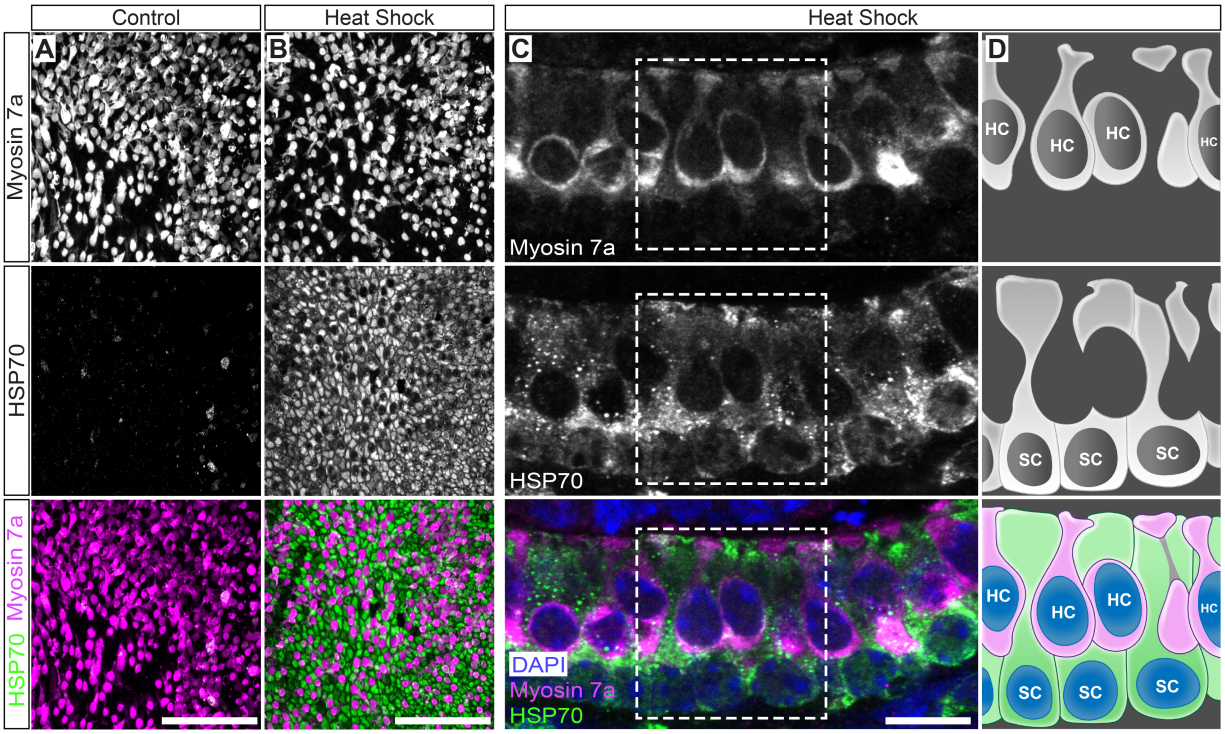

Figure 1:
HSP70 is upregulated in supporting cells upon heat shock. Mouse utricles were cultured under control or heat shock conditions, fixed 6 hours later and labeled with antibodies against Myosin 7a (hair cell marker, magenta) and inducible HSP70 (green). **(A-B)** Confocal images of whole-mount utricles show sensory hair cells surrounded by glia-like supporting cells. **(A)** Inducible HSP70 is not detected under control culture conditions. **(B)** Heat shock induces HSP70 specifically in supporting cells, with very little induction in hair cells. **(C)** Cryosection of a heat-shocked utricle confirms negligible induction of HSP70 (green) in hair cells (labeled with Myosin 7a, magenta), while HSP70 is substantially upregulated in supporting cells. Nuclei in (A-C) were stained with DAPI (blue). **(D)** Schematics showing locations of hair cells (HC, magenta) and supporting cells (SC, green) in boxes outlined in (C), with nuclei indicated in blue in lower right panel. Scale bars = 50 μm in A-B; 10 μm in C.

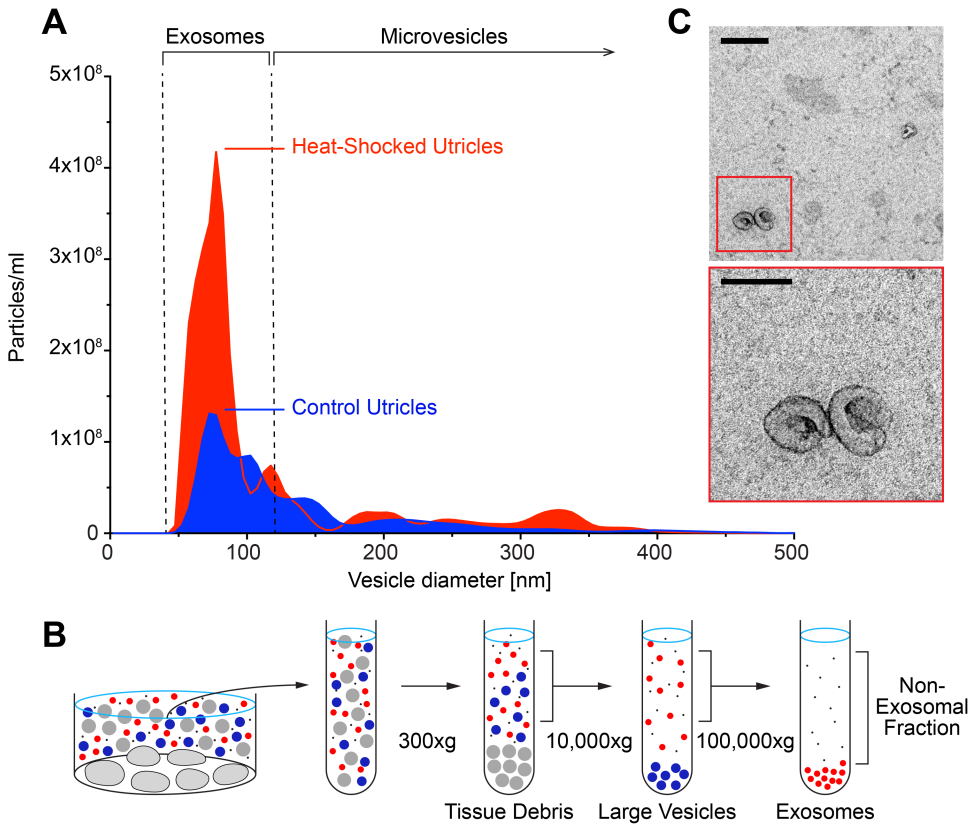

Figure 2:

Heat stress stimulates exosome release from inner ear tissue. (A) Nanoparticle tracking analysis of conditioned media from utricles cultured under control conditions shows release of exosome-sized (~50-150 nm diameter) particles from control utricles. Heat shock results in a 2.4-fold increase in exosome release. Brackets denote typical size ranges of exosomes and microvesicles. **(B)** Schematic of differential ultracentrifugation procedure used to isolate exosomes from utricle-conditioned culture medium. This process sequentially sediments extracellular components of decreasing size (tissue debris - grey; large vesicles - blue), with exosomes (red) isolated in the final pellet. **(C)** Isolated exosomes from utricle-conditioned media visualized by transmission electron microscopy (TEM) were ~90 nm in diameter and displayed canonical cup-shape morphology. Red box in top panel denotes area shown at higher magnification in bottom panel. Scale bars: top panel, 200 nm; bottom panel, 100 nm.

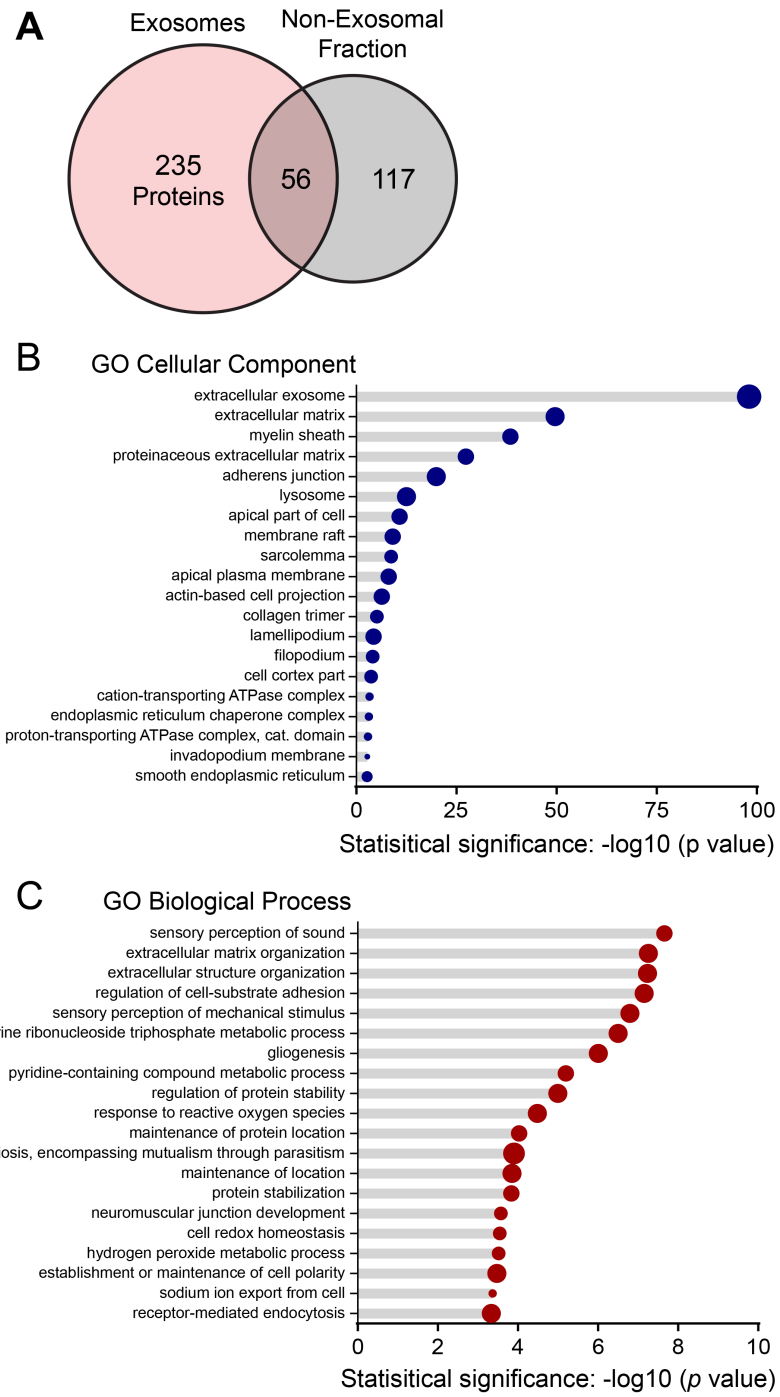

Figure 3:
Proteins identified in utricle exosomes. Proteins associated with exosomes and non-exosomal proteins secreted from heat-shocked utricles were identified using tandem mass spectrometry. Exosomes were isolated from conditioned media via size exclusion chromatography and analyzed in parallel with the exosome-depleted media ("non-exosomal fraction"). **(A)** 291 unique protein families were identified in exosomes, 56 of which were also found in the non-exosomal fraction. **(B)** The twenty most significantly enriched gene ontology (GO) cellular component terms for proteins identified in utricle-derived exosomes. **(C)** The twenty most significantly enriched biological process GO terms for proteins identified in exosomes from utricles.

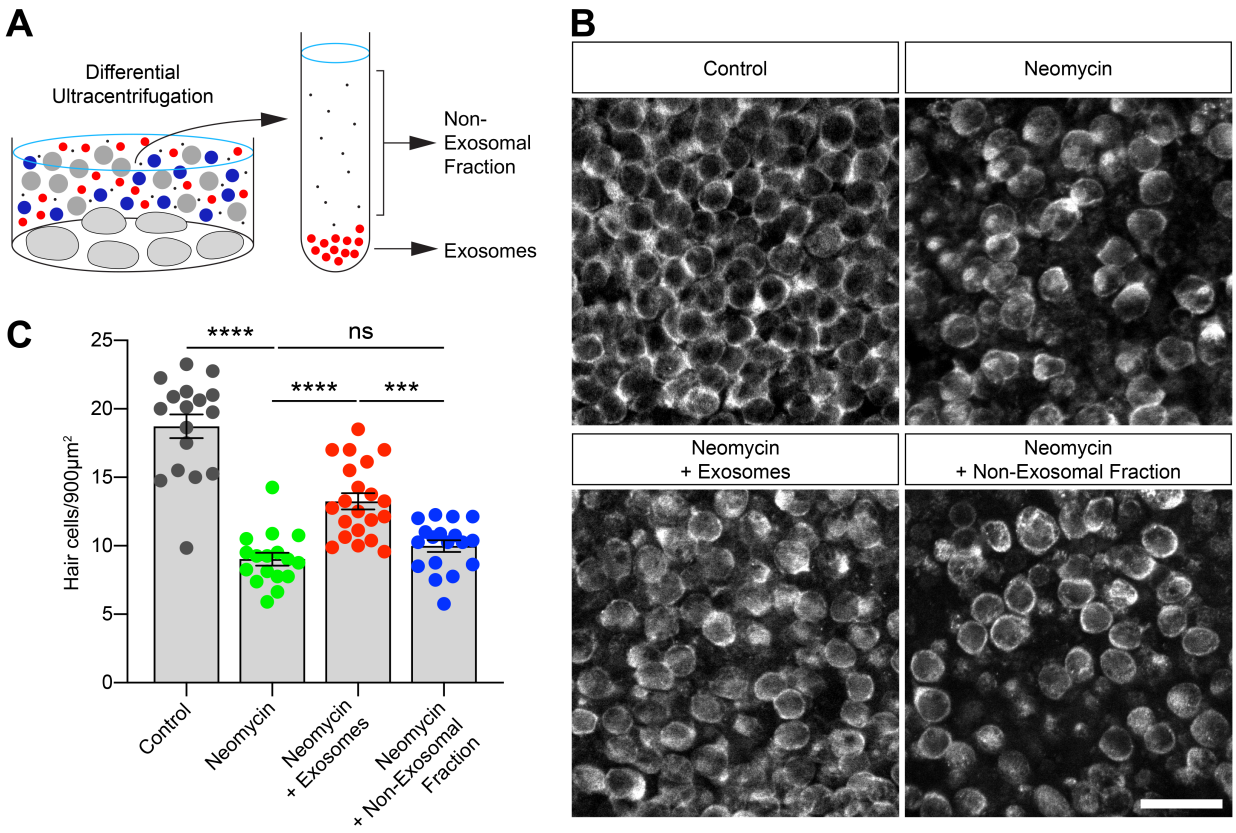

Figure 4:
Isolated exosomes protect against neomycin-induced hair cell death. Utricles were cultured for 24 hours in neomycin, with or without the addition of exosomes isolated from heat-shocked utricles. **(A)** Exosomes and the non-exosomal fraction (supernatant) were purified from utricle-conditioned media using differential ultracentrifugation (see Figure 2B) and applied to neomycin-treated utricles. **(B)** Fixed utricles were labeled with the hair cell marker myosin 7a, and images were acquired using laser scanning confocal microscopy. Representative z-sections from surface preparations of utricle whole-mounts are shown. Scale bar, 20 μm. **(C)** Neomycin caused hair cell death. Application of isolated exosomes significantly improved hair cell survival. In contrast, no protective effect was observed when the non-exosomal fraction (i.e., exosome-depleted conditioned media) was added. Each data point represents the average hair cell density of an individual utricle. n = 16-20 utricles per condition from four independent experiments. Error bars represent mean ± SEM. ***$p < 0.001$, ****$p < 0.0001$, ns = not significant as determined by Brown-Forsythe and Welsh ANOVA followed by Dunnett's T3 multiple comparisons test.

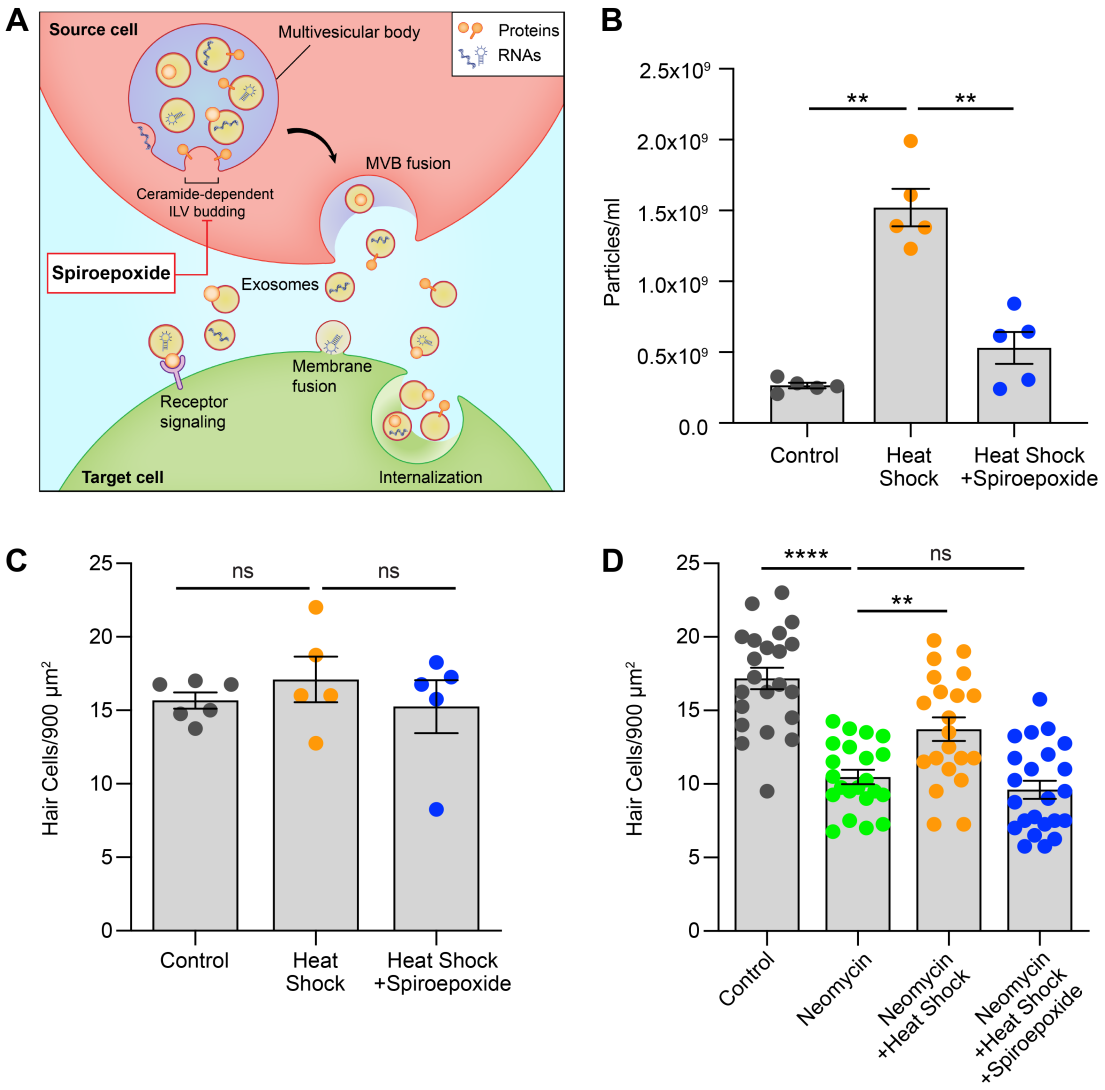

Figure 5:
Exosomes are required for the protective effect of heat shock. (A) Exosomes containing proteins, nucleic acids, and lipids are released from source cells (red) and can modify the biological state of target cells (green) via a variety of interactions. Within the source cell, exosome biogenesis occurs via budding of intraluminal vesicles (ILVs) into the lumen of a multivesicular body (MVB, purple), a process that requires the sphingolipid ceramide. The neutral sphingomyelinase II inhibitor spiroepoxide blocks ceramide production and inhibits exosome biogenesis. **(B)** Inhibition of exosome biogenesis reduces the number of exosome-sized particles in conditioned media from heat-shocked utricles. Data are presented as mean ± SEM for five NTA captures. **(C)** Quantification of surviving hair cells in utricles demonstrated that reduced exosome release in the presence of spiroepoxide is not caused by cytotoxicity. n = 5-6 utricles per condition. **(D)** Utricles were cultured for 24 hours in neomycin, with or without heat shock and with or without spiroepoxide. Neomycin caused hair cell death, while heat shock improved survival of neomycin-exposed hair cells. Inhibition of exosome biogenesis using spiroepoxide abolished the protective effect of heat shock. n = 21-23 utricles (shown as individual data points) per condition. Error bars represent mean ± SEM. $^{**}p < 0.01$, $^{****}p < 0.0001$, ns = not significant as determined by Brown-Forsythe and Welsh ANOVA followed by Dunnett's T3 multiple comparisons test (B, D) or One-way ANOVA followed by Holm-Šídák multiple comparisons test (C).

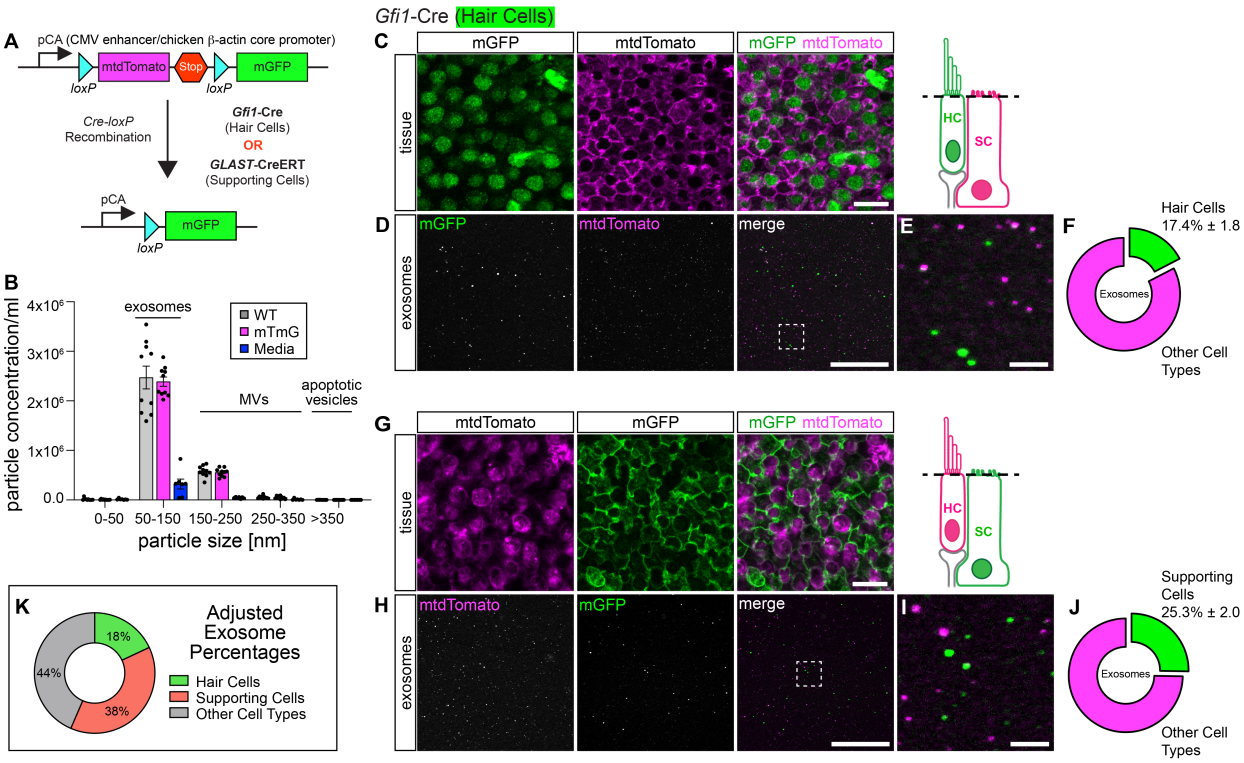

Figure 6:

Supporting cells release more exosomes than hair cells under heat stress. (A) mTmG double-fluorescent reporter mice constitutively express myristoylated tdTomato. When crossed to Cre recombinase expressing mice, the *loxP*-flanked mtdTomato cassette is deleted in all *cre* expressing cells, resulting in tissue-specific mGFP fluorescence. **(B)** NTA of conditioned media from heat-shocked utricles of mTmG mice (magenta) or age-matched wild-type (WT) mice (grey) shows that lipidation of fluorophores in mTmG mice does not affect exosome release. The culture media (blue) contributed 10% of particles to each size category. MVs, microvesicles. Data are presented as mean ± SEM from two independent experiments (n = five NTA captures from 22 utricles for each condition). **(C)** Utricles from mTmG mice crossed to *Gfi1*-Cre mice display mGFP-expressing hair cells (green), while supporting cells retained mtdTomato expression (magenta). Schematic indicates focal plane. HC, hair cell; SC, supporting cell. **(D)** Fluorescence emitted from utricle-derived exosomes from mTmG mice crossed to *Gfi1*-Cre mice. Box indicates region magnified in **(E)**. **(F)** 17.4% of utricle-derived exosomes depicted in (D) were mGFP-positive. **(G)** Supporting cells in mTmG mice crossed to *GLAST*-CreER mice were mGFP-positive (green). All other cells retained mtdTomato expression (magenta). **(H)** Fluorescence emitted from utricle-derived exosomes from mTmG mice crossed to *GLAST*-CreER mice. Box indicates region magnified in **(I)**. **(J)** 25.3% of exosomes visualized in (H) were mGFP-positive. **(K)** Contributions of hair cells and supporting cells to the total utricle-derived exosome population after taking Cre recombinase efficiency in hair cells (*Gfi1*-Cre = 96.5%) and supporting cells (*GLAST*-CreER = 64.5%) into account. 44% of exosomes were likely contributed by other cell types. Results in F and J are presented as mean ± SEM from three experiments (n = 9-11 utricles per condition). Scale bars, 10 μm in C, G; 50 μm in D, H; 5 μm in E, I.

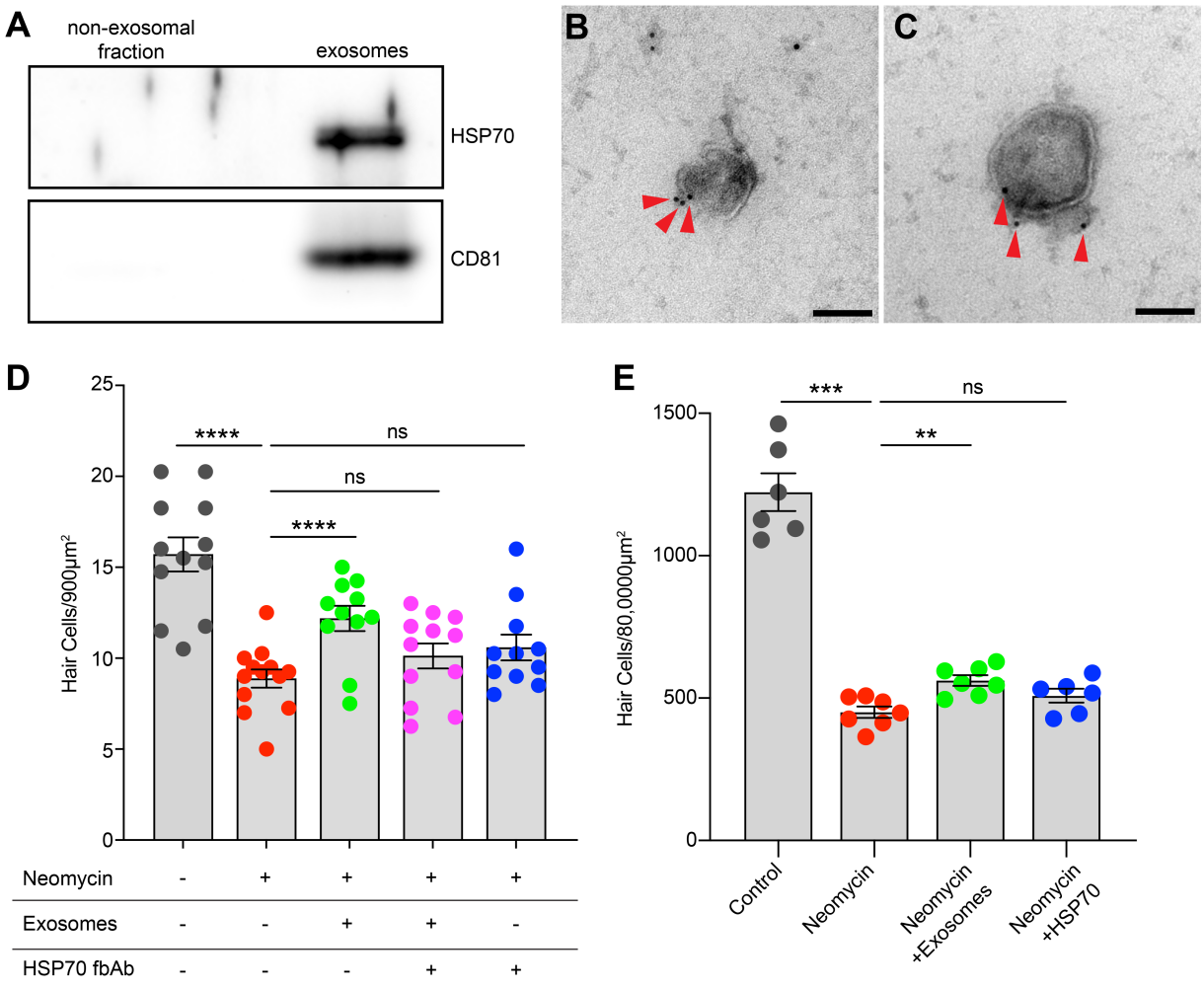

Figure 7:
Exosomes contain HSP70, and exosome-associated HSP70 is required for the protective effect of exosomes. (A) Western Blot shows association of HSP70 with exosomes but not the non-exosomal fraction. Similarly, CD81 (exosome marker) is detected exclusively in exosomes. Exosomes and the non-exosomal fraction were isolated from heat-shocked utricles by differential ultracentrifugation (Figure 2B). Equivalent total protein amounts were loaded per lane. **(B, C)** Two representative immunogold TEM micrographs of utricle-derived exosomes reveal HSP70 immunoreactivity (red arrowheads) near the exosomal membrane. Scale bars, 100 nm. **(D)** HSP70 is required for the protective effect of exosomes. Utricles were cultured for 24 hours in the presence of neomycin, with or without the addition of exosomes isolated from heat-shocked utricles. Exosomes significantly protected hair cells against neomycin ototoxicity. Addition of an HSP70 function-blocking antibody (fbAb) abolished the protective effect of exosomes. Each data point represents the average hair cell density of an individual utricle from four independent experiments (n = 11-13 utricles per condition). **(E)** Non-exosomal HSP70 is not protective against neomycin-induced hair cell death. Utricles were cultured for 24 hours in the presence of neomycin, with the addition of either isolated exosomes or soluble (recombinant, non-exosomal) HSP70. Exogenous HSP70 failed to protect hair cells, while exosomes were protective. Error bars represent mean ± SEM. $^{**}p < 0.01$, $^{***}p < 0.001$, $^{****}p < 0.0001$, ns; not significant as determined by Brown-Forsythe and Welsh ANOVA followed by Dunnett's T3 multiple comparisons test.

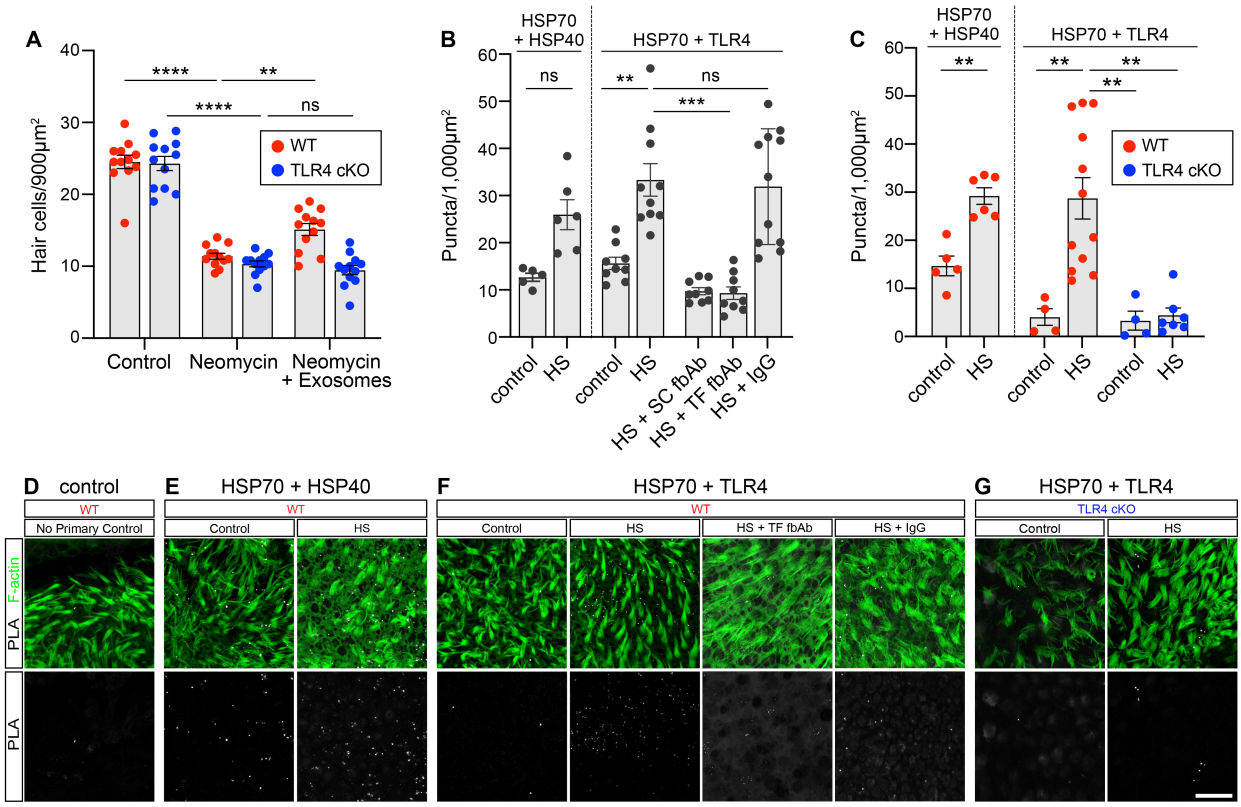

Figure 8:

The protective effect of exosomes requires interaction of exosomal HSP70 with TLR4 on hair cells. **(A)** Exosomes improve hair cell survival in neomycin-exposed utricles from control littermates (WT, red) but not from hair-cell-specific TLR4 conditional knock-out (cKO) mice (blue). Data are mean ± SEM (n = 12 utricles per condition). $^{**}p < 0.01$, $^{****}p < 0.0001$, ns; not significant as determined by Two-way ANOVA followed by Holm-Šídák multiple comparisons test. **(B-C)** A proximity ligation assay (PLA) was used to detect interaction between exosomal HSP70 and HSP40 or HSP70 and TLR4. **(B)** Two different function-blocking antibodies (fbAB; SC, Santa Cruz; TF, ThermoFisher) against HSP70 abolished the interaction between HSP70 and TLR4, while IgG had no effect. **(C)** Heat shock increased the interaction between HSP70 and HSP40 and between HSP70 and TLR4 in WT utricles. Hair-cell-specific deletion of TLR4 abolished the PLA signal in heat-shocked utricles from TLR4 cKO mice. Data in B-C are mean ± SEM, shown as average puncta per 1,000 µm^2 (n = 4-12 utricles per condition). $^{**}p < 0.01$, $^{***}p < 0.001$, ns; not significant as determined by Brown-Forsythe and Welsh ANOVA followed by Dunnett's T3 multiple comparisons test. **(D-G)** Confocal images of PLA signals in utricles from (D-F) WT or (G) TLR4 cKO mice under control or heat shock conditions. Top row, F-actin (green) and PLA signal (white); bottom row, PLA signal only (white). **(D)** Negative control (no primary antibody). **(E)** Heat shock induces HSP70 interaction with HSP40 in WT utricles. **(F)** Heat shock increases HSP70 interaction with TLR4 in WT utricles. Function-blocking antibodies (HSP70 fbAb) inhibit interaction between HSP70 and TLR4 in WT utricles, independently of heat shock, whereas control IgG has no effect. **(G)** Hair-cell specific deletion of TLR4 abolishes the HSP70-TLR4 interaction in TLR4 cKO mice. Scale bar, 20 µm.

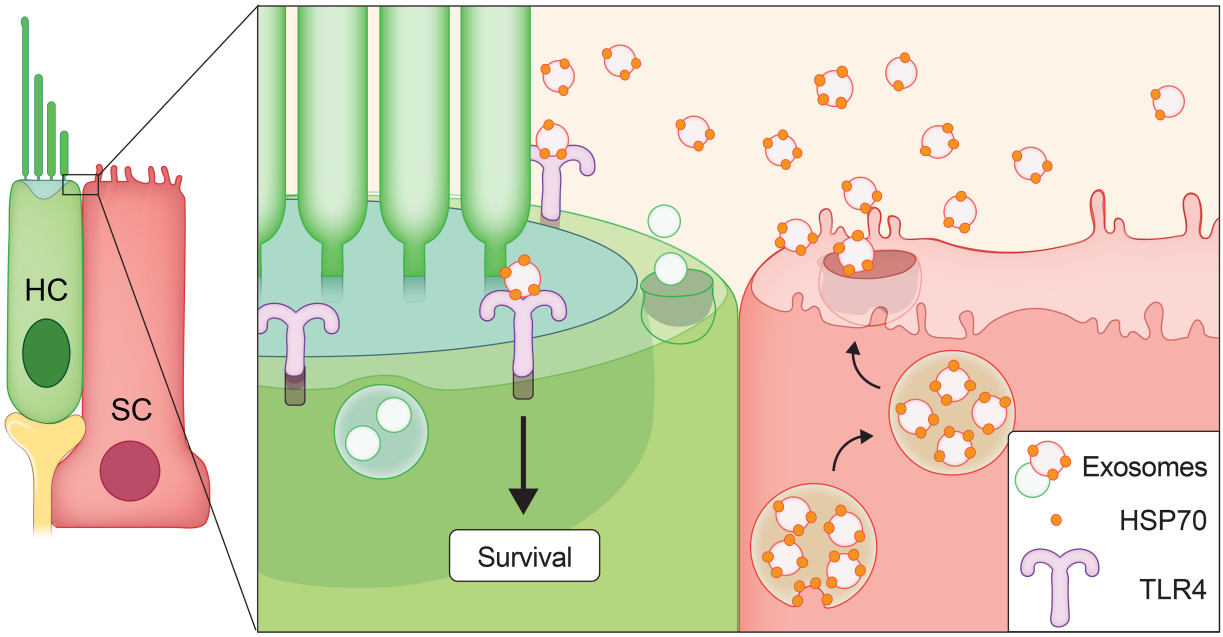

Figure 9:
Model for the role of exosomes as mediators of protection against hair cell death caused by ototoxic drugs.
Our data are consistent with a model in which heat stress induces HSP70 expression, predominately in supporting cells (Figure 1). Some of this HSP70 associates with exosomes (Table 1, Figure 7A-B) that are released into the extracellular environment (Figures 2A, 5B). HSP70-carrying exosomes interact with TLR4 on the hair cell surface (Figure 8) to stimulate a pro-survival response (Figures 4B-C, 5D). The significance of hair cell-derived exosomes (Figure 6C-K) remains under investigation.

Table 1:
Proteins commonly used as exosome markers were confirmed in the utricle-derived exosome fraction but not in the non-exosomal fraction.

Common Exosome Markers		
Protein (Gene Symbol)	**Exosomes**	**Non-Exosomal Fraction**
CD9 antigen (*Cd9*)	+	-
CD81 antigen (*Cd81*)	+	-
CD63 antigen (*Cd63*)	+	-
Tumor susceptibility gene 101 (*Tsg101*)	+	-
Programmed cell death 6 interacting protein (*Alix*)	+	-
Heat shock 70 kDa protein family	++	+

Table 2:
Integrin subunits identified in utricle-derived exosomes. Gene symbols are listed in parentheses.

Exosome-Associated Integrins	
Alpha Subunits	**Beta Subunits**
alpha 3 (*Itga3*)	beta 1 (*Itgb1*)
alpha 7 (*Itga7*)	
alpha V (*Itgav*)	